A. Airoldi, C. Mirani, L. Principito
A Bi-Phasic Modelling Approach for Interlaminar and Intralaminar Damage in the Matrix of Composite Laminates
Composite Structures, In press - Published online 29/11/2019
doi:10.1016/j.compstruct.2019.111747

A bi-phasic modelling approach for interlaminar and intralaminar damage in the matrix of composite laminates

Alessandro Airoldi[1], Chiara Mirani[1], Lucia Principito[1]

[1]*Dept. of Aerospace Science and Technology, Politecnico di Milano*
Via La Masa 34, 20156 – Milano - ITALY
Email: alessandro.airoldi@polimi.it

Abstract

The paper presents a new bi-phasic approach to model delamination and transverse cracking in the matrix of composite laminates by using a single constitutive law, based on a decomposition of the composite stiffness properties into idealized fibre and matrix phases. The decomposition is used in finite element models where membrane elements representing the fibre phase are embedded in a three-dimensional mesh that models the matrix phase. A single constitutive law is applied to the matrix phase by combining a Cohesive Zone Model, which models delamination between plies, with an intralaminar damage law, aimed at modelling a transverse matrix cracking within the plies. All the theoretical aspects of decomposition and constitutive law are described. Then, the numerical experimental correlations are presented considering delamination tests and the evolution of the transverse matrix cracking in cross-ply specimens, with a statistical distribution of strength properties, also in the presence of interactions between matrix cracking and delamination. The approach provides the possibility to efficiently simulate both individual delaminations and transverse cracks with a model using a single layer of elements per ply, without introducing interface elements. Moreover, it also provides new possibilities to control the interaction between intralaminar and interlaminar damage phenomena.

Keywords: Composite Damage; Delamination; Transverse Matrix Cracking; FE models; Bi-phasic models; Damage Modes Interaction

1. Introduction

The application of long fibre reinforced composites in primary structures of aerospace and high performance vehicles has been motivated by their structural efficiency and technological advantages. However, it is necessary to face several critical issues related to the occurrence of multiple types of damage, which affect the structural integrity at various degrees [1].

An important distinction can be introduced between the damage evolving in the matrix and fibre breakages. Indeed, fibre breakage represents a more immediate threat to the integrity of the composite part and cannot be tolerated. On the contrary, damages in the matrix of composite plies is typically characterized by a progressive accumulation, which starts at load levels significantly lower than the maximum ones carried by laminates [2–5]. Delamination is also a damage in the matrix of composite, which is initially originated as a consequence of specific events such as impacts or defects developed during the manufacturing process [6]. After the onset, also delamination evolves in a progressive way under the action of operational loads and is tolerated within certain limits in modern design approaches, although it leads to a reduction of the laminate strength. In general, the evolution of matrix damage affects stiffness properties, stress distributions, strength and the residual strength of laminates. Therefore, the modelling of such damage is fundamental to predict the mechanical response of composites and to numerically support the application of the damage tolerance design philosophy [7,8].

The aim of this paper is to present an innovative modelling technique based on a bi-phasic decomposition of the composite material into idealized fibre and matrix phases, allowing to describe different types of matrix damage with a unique constitutive law and to develop computationally efficient models.

A large number of approaches have been proposed in literature to model different types of matrix damage, at different scales of observation. With regard to intralaminar damage, thermodynamically consistent approaches based on Continuum Damage Mechanics (CDM) have been suggested by many authors to model stiffness degradation due to matrix cracking, at the level of the homogenized sub-

laminate, ply or sub-ply level [9]. The orthotropy of composite plies has been exploited by introducing several scalar damage variables, which separately affect the engineering constants that characterize matrix- and fibre- dominated properties [10–16]. More refined models based on a physical consideration or linked to micromechanical approaches are also available [17–20].

There is also a special class of bi-phasic approaches that decompose the composite materials into fibre and matrix phases, to emphasize the differences and the effects of damages in matrix-dominated and in the fibre-dominated response of composite materials. Examples are represented by bi-phasic models proposed in [21–24] , for polymer matrix composites, which were applied to model intralaminar damage for crashworthiness applications. Actually, the phases defined in these models should be properly defined as idealized phases, since they occupy the same volume and do not represent the physical constituent materials, occupying separated volumes and subjected to different strain states. The idealized phases have constitutive laws that provide separate stress contributions but depend on the average strain state in the composite at the homogenized ply level.

The advantages claimed by the bi-phasic point of view are related to the possibility to model matrix degradation with a separate constitutive law, including, for instance, the modelling of matrix damage due to stress components acting in reinforcement direction, which can be experimentally measured [25]. The results reported in [24] show that non-linear response and the evolution of Poisson's ratio can be captured in angle ply carbon and glass reinforced laminates $[+\vartheta/-+\vartheta]_s$ with unidirectional and fabric reinforcement for many values of ϑ, by using a single damage variable. Other examples of decomposition of composite properties into superimposed phases are represented by the binary models developed in [26–28] for ceramic matrix composites, where matrix-dominated non linearity is modelled with a constitutive law written for an effective continuum medium that embeds a reinforcement phase. However, it should be observed that a fundamental issue for the application of bi-phasic or binary models is the development of adequate procedures for decomposition. In particular, decomposition procedures that can lead to non-physically admissible matrix phases should be avoided, as highlighted in [24]. Although the approach presented in this paper exploits the bi-phasic decomposition in a different way

than the approaches presented in the previous works, the issues related to decomposition procedure have to be solved.

Delamination is another type of matrix damage that has been intensively studied in the last decades. In recent years, delamination has been often modelled by representing the individual cracks, even in relatively coarse meso-scale models, by using zero-thickness cohesive elements set at interfaces between the plies, modelled by three-dimensional solid elements [29]. Cohesive elements are based on Cohesive Zone Models (CZM) that allow to represent both the strength and the toughness of interlaminar layers [30,31]. Before crack onset, cohesive elements are required to model a perfect adhesion between the adjacent layers, so that they have to be characterized by a very high penalty stiffness, which is known to cause numerical problems [32–34]. An alternative modelling technique to overcome such problems was discussed and validated in [35,36], where a CZM was included into finite thickness elements, as done in [37–40] to model interlaminar resin reach layers and adhesive films. In the approach proposed in [35,36], a CZM for delamination was embedded into three-dimensional elements with finite thickness, which carried only out-of-plane stress states. Such elements were used to connect layers representing the plies, modelled by shell or membrane elements, that is by elements with a two-dimensional geometry. Owing to the different elements adopted in the mesh, the technique was called hybrid modelling technique. The embedment of CZM into finite thickness elements was found to be particularly suited for the application in quasi-static explicit analyses of delamination phenomena, which are useful to easily model complex damage scenarios (see for instance [35,36,41–44]). Indeed, explicit analyses are severely penalized by a reduction of stable time integration steps due to the presence of very stiff elements [36,45]. Therefore, the adoption of traditional zero-thickness cohesive elements can lead to very large computational times and other numerical issues. On the contrary, the modelling approach based on finite thickness elements can be used to develop reliable and computationally efficient models, [30, 31,36–39].

The above mentioned studies present some of the approaches used to model damage in the matrix of composite laminates. However, it should be observed that, in all the considered works, intralaminar and interlaminar damage were modelled by using separate constitutive laws, which can be used in the elements representing the ply and in the cohesive elements introduced to model delamination, as in[46,47]. Nevertheless, both types of damage are different forms of matrix damage and they are characterized by significant interactions, since intralaminar cracks are known to be an important cause for the development of delamination [47–50]. These interactions can be modelled by developing finite element models refined at the sub-ply level, with more than ten elements through the thickness of the layers where intralaminar cracks develop, such as in [3,15]. Alternatively, meso-scale models can be linked to micro-mechanical approaches [19,51]. In general, the studies presented in literature indicate that the intra-interlaminar interaction can be captured by representing in detail the stress state in the vicinity of individual intralaminar matrix cracks. However, this cannot be easily carried out in meso-scale models, where each ply is represented by a single layer of solid elements, since meshes are too coarse to represent the through-the-thickness stress gradients and the interlaminar shear stress distribution close to transverse cracks. Moreover, the complete opening of a transverse crack in a layer is opposed by the confinement effect of adjacent layers with different fibre orientations, as discussed in [52]. Despite such difficulties, interactions have been represented in meso-scale models with the application of extended finite element methods [53,54] or the interposition of cohesive elements in the mesh of the plies to represent pre-defined locations for individual intralaminar matrix cracks [52,55,56]. Other approaches have eliminated the need to model individual intralaminar cracks, as in [16] where a non-local finite element procedure was used, and the parameters of the cohesive zone model in the interlaminar layer were influenced by the intralaminar damage state in the adjacent plies. A similar approach was adopted in models of laminates based on high order shell elements, which are capable to capture the complete three-dimensional stress states at each single through-the-thickness integration point [57].

This work developed a bi-phasic meso-scale model for composite laminates by combining the modelling technique approach for delamination, presented in [35,36], and a bi-phasic decomposition of composite properties ([23,24]). All types of matrix damage are represented within a single constitutive law attributed to a matrix idealized phase modelled by three-dimensional elements that connect layers of two-dimensional elements representing the fibre phase. Such approach retains the computational advantages related to the elimination of penalty stiffness in the analyses of delamination, shown in [35,36,41–44]. Moreover, it allows to model intralaminar damage at different levels of detail, even including the possibility to describe individual matrix cracks. Indeed, this study shows that the modelling technique inherently reduces the problems related to the confinement effects of the adjacent plies on the opening of transverse matrix cracking. Finally, it allows to adopt different strategies to control the interactions between intralaminar damage and delamination.

The following Section of this paper presents the basic ingredients of the numerical bi-phasic model proposed. Moreover, it introduces a new and robust bi-phasic decomposition algorithm for three-dimensional stress states aimed at overcoming the shortages outlined in [24]. Section 3 develops the structure of the constitutive law attributed to the matrix phase. Section 4 and Section 5 are dedicated to the application and validation of the model. Specifically, Section 4 describes the correlation between mode I and mode II delamination tests, and includes an estimation of computational advantages with respect to more conventional approaches. Section 5, instead, shows how individual transverse matrix cracks within the plies can be represented thanks to the specific aspects of the technique, and assesses the possibility to represent the evolution of transverse crack densities by using a statistical distribution of matrix strength properties. The cases considered include situations where the interaction between intralaminar and interlaminar damage significantly affects the results. Finally, Section 6 provides concluding remarks summarizing the main findings of the activity presented in this paper.

2. Fundamental aspects of the modelling approach

2.1 Original hybrid technique to model delamination by using finite thickness connection elements

The approach developed in this paper moves from the modelling technique developed and applied in [35,36,41–44] for delamination, which is described and compared with a more conventional approach in Fig. 1. This original modelling technique was referred to as a hybrid technique in the published papers due to the adoption of different types of elements to mesh composite laminates at the ply level. The laminate was seen as an assembly of plies represented separately by a mesh of membrane elements, with two-dimensional geometry, with nodes set at the mid-planes of the plies. Such layers of two-dimensional elements carried the in-plane stress components acting in the plies. The membrane elements modelled the in-plane stress response of the plies, and were characterized by the total thickness of the ply the modelled. They were mutually connected by three-dimensional elements, which modelled only the response of the laminate to the average out-of-plane strain state, in the volume between the mid-planes of the two adjacent plies [35]. The two types of elements occupied the same volume and provided different stress contributions.

Trilinear hexahedral elements with a reduced integration scheme were used as three-dimensional elements, for the out-of-plane response. They were characterized with a null in-plane response and with the physical out-of-plane stiffness parameters of the material. Compatibility between displacements at the mid-plane of plies was assured by the use of linear interpolation schemes for both types of elements. The validation of this unconventional modelling technique was presented in [30, 31] with comparison with reference models with different lay-ups.

The interlaminar fracture process was described in the three-dimensional elements as a function of a vector of relative displacements between the mid-planes of two adjacent plies, U^L and U^U. This vector was linked to the average out-of-plane strain state, evaluated at the single integration point of the hexahedral elements, $\{\varepsilon_{zz}\ \gamma_{yz}\ \gamma_{xz}\}$, under the assumption of infinitesimal strains. Thanks to such link, a

CZM was expressed in terms of strain-strain relation and embedded into the finite thickness three dimensional elements, as described in [35,36] and represented in Fig. 1. The prediction of internal strain states given by using this approach to model stable fracture propagation in mode I and mode II were validated by means of embedded sensors carried by optical fibres in [31]. The advantages of the approach, which was used to reliably model complex delamination scenarios in composite laminates, are summarized in the following points:

(i) elimination of duplicated degrees of freedom at the interfaces;

(ii) elimination of the need to calibrate penalty stiffness, since out-of-plane physical stiffness properties of the material are used;

(iii) significant increment of minimum stable time steps in explicit analyses, due to the absence of zero or infinitesimal thickness elements;

(iv) suitability to easily model the friction between interlaminar layers after crack development, which can represent an additional force opposing to crack development.

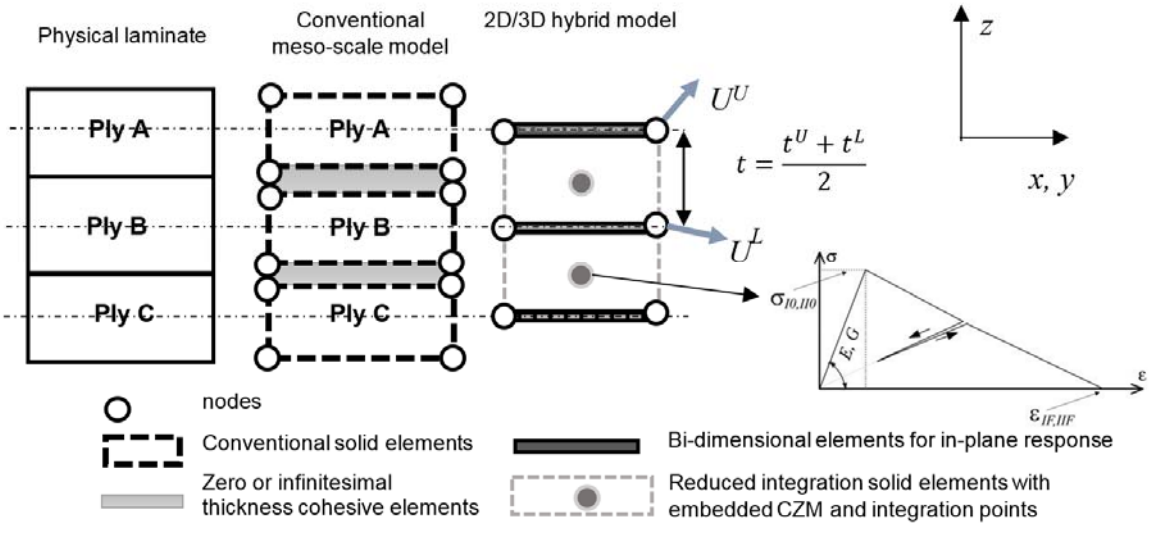

Fig. 1 – Conventional technique and hybrid modelling technique for meso-scale models

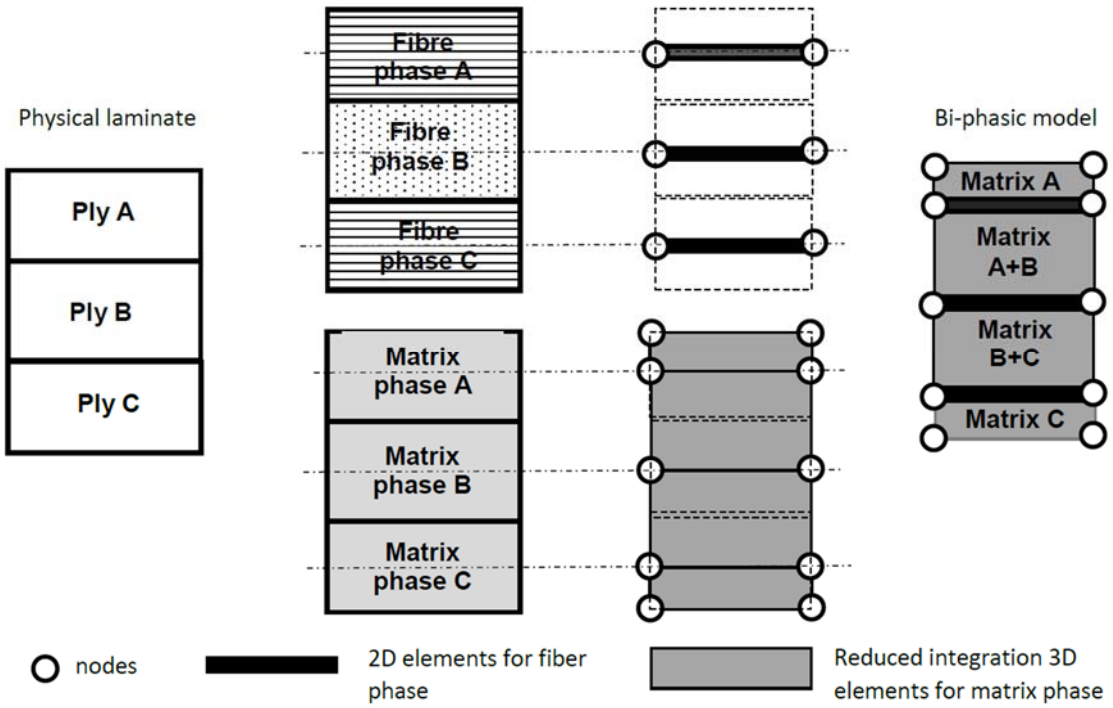

Fig. 2 – Scheme of the bi-phasic model

2.2 Basic aspects of bi-phasic approaches

In this paper, the hybrid technique represented in Fig. 1 is adopted and modified to represent a bi-phasic model of the composite laminate, where the response of the composite is obtained by summing the stress contribution of two idealized phases, modelling fibre-dominated and matrix-dominated responses, respectively.

In the bi-phasic model, which is not a micromechanical approach, the total stress state in the composite material is represented by vector $\boldsymbol{\sigma}^C$, which is the sum of two superimposed phases sharing the same volume. Such phases are the idealized phases of the fibre and matrix, and their stress contributions are represented by stress vectors $\boldsymbol{\sigma}^f$ and $\boldsymbol{\sigma}^m$. The responses of the idealized phases are characterized by a constitutive response defined on the basis of the strain in the composite ply, averaged at the homogenized material level, as shown in Eq. 1.

$$\boldsymbol{\sigma}^c = \boldsymbol{\sigma}^f + \boldsymbol{\sigma}^m = \boldsymbol{D}^c\boldsymbol{\varepsilon} = \left(\boldsymbol{D}^f + \boldsymbol{D}^m\right)\boldsymbol{\varepsilon} \quad \text{Eq.1}$$

where $\boldsymbol{D}^f$ and $\boldsymbol{D}^m$ are the stiffness matrices that characterize the constitutive response of the fibre and matrix phases, respectively, and $\boldsymbol{D}^c$ is the stiffness matrix of the composite. The decomposition is performed considering the local reference frame for the orthotropic material, with axes 1 and 2 in the plane of the laminate material.

The decomposition is actually functional to describe different types of damage at the homogenized ply level, so it is possible to define the idealized phases in several ways, without affecting the response of the homogenized composite model to the average strain in elastic range. There is no need of simplifying assumptions about the local strain states experienced by the phases, since the only strain considered in the average strain in the composite at the homogenized ply level. The simplest way to apply this decomposition in order to separate the description of non-linearity in fibre- and matrix-dominated response is to define an idealized fibre phase that carries only normal stress in the reinforcement directions and represent the effect of fibre continuity. The fibre stiffness matrix in a bi-phasic model may be evaluated by defining an effective fibre modulus, $E^{f\text{-}eff}$, and the fibre volumetric fraction, V^f [21–24].. The stiffness terms of the matrix phase provide all the remaining contributions to the overall stress state. Therefore, the response in the elastic range is expressed as in Eq. 2, which is referred to a ply with unidirectional reinforcement:

$$\begin{Bmatrix}\sigma_{11}\\ \sigma_{22}\\ \sigma_{33}\\ \tau_{12}\\ \tau_{23}\\ \tau_{31}\end{Bmatrix} = \left(\begin{bmatrix}E^{f-eff}V^f & 0 & 0 & 0 & 0 & 0\\ 0 & 0 & 0 & 0 & 0 & 0\\ 0 & 0 & 0 & 0 & 0 & 0\\ 0 & 0 & 0 & 0 & 0 & 0\\ 0 & 0 & 0 & 0 & 0 & 0\\ 0 & 0 & 0 & 0 & 0 & 0\end{bmatrix} + \begin{bmatrix}D_{11}^m & D_{12}^m & D_{13}^m & 0 & 0 & 0\\ D_{21}^m & D_{22}^m & D_{23}^m & 0 & 0 & 0\\ D_{31}^m & D_{32}^m & D_{33}^m & 0 & 0 & 0\\ 0 & 0 & 0 & D_{44}^m & 0 & 0\\ 0 & 0 & 0 & 0 & D_{55}^m & 0\\ 0 & 0 & 0 & 0 & 0 & D_{66}^m\end{bmatrix}\right) \begin{Bmatrix}\varepsilon_{11}\\ \varepsilon_{22}\\ \varepsilon_{33}\\ \gamma_{12}\\ \gamma_{23}\\ \gamma_{31}\end{Bmatrix} \quad \text{Eq. 2}$$

If the effective fibre modulus and the fibre volumetric fractions are known, the stiffness terms of the idealized matrix phase can be obtained by subtracting the fibre contribution from the composite stiffness matrix, which is assumed known from experimental characterization:

$$\boldsymbol{D}^m = \boldsymbol{D}^c - \boldsymbol{D}^f \quad \text{Eq. 3}$$

The strategy adopted to develop the binary models described in [26-28] is very similar and it is motivated by the need of a computationally efficient method to model matrix dominated non linearity. It should be remarked that the idealized fibre phase should be considered more representative of fibre continuity, rather than of the physical material constituting the reinforcement. Indeed, the response of matrix phase includes the properties of the fibres in direction different from the orientation one. Accordingly, matrix can be considered an effective continuum medium [26-28], with properties related to the physical matrix, but which actually represents composite properties without fibre continuity. An algorithm to perform the decomposition, consistent with the aforementioned considerations, is introduced in section 2.4.

2.3 Bi-phasic model for a composite laminate subjected to three-dimensional stress states

In this work, the bi-phasic decomposition is incorporated in the hybrid technique shown in Fig. 1, to make possible the representation of all matrix-dominated inelastic responses, related to intralaminar and interlaminar damage by using a single constitutive law. Indeed, in the bi-phasic model presented in this

paper, the two-dimensional elements are characterized with the properties of the idealized fibre phase, whereas the three-dimensional elements are characterized by a constitutive law that represented the whole contribution of the idealized matrix phase.

The resulting model, presented in Fig. 2, can be described as a fibre phase mesh, represented by two-dimensional elements, which will be referred to as 2D elements, with nodes at the mid-planes of the plies, embedded into a solid mesh modelling the matrix phase, constituted by three-dimensional elements connecting the mid-planes of the plies, which will be referred to as 3D elements. The binary models developed and applied in [26–28] for textile composites also adopt different types of elements, since the properties of reinforcement are attributed to 1D elements embedded in a solid mesh representing an effective continuum medium.

In the model presented in this paper, each 3D element actually represents the matrix phase of two adjacent plies, as highlighted in Fig. 2, with the exception of the elements at the laminate surface. Following the original approach shown in Fig. 1, the out-of-plane strain state in the 3D elements can be related to the separation of the plies and a CZM is introduced to model delamination, as shown in Section 3. Moreover, the same constitutive law used in the 3D elements is also suited to model a matrix-dominated in-plane response, including intralaminar damage, by using a CDM approach. This allows to model these two types of matrix damage within a single constitutive model. The expected advantages of the approach are summarized in the following points:

(i) all the advantages of the original hybrid technique in modelling delamination are retained;

(ii) the approach offers a particular and appealing point of view to model both interlaminar and intralaminar matrix damage in the same constitutive law, and to better control their interactions;

(iii) individual matrix cracking with a mesh at the meso-scale level can be represented, as shown in Section 5, since the modelling technique attenuates significantly the confinement effect of adjacent plies with different fibre orientations, discussed in [52];

(iv) the potential advantages offered by bi-phasic approach can be exploited to write constitutive law specialized to represent matrix-dominated non-linearity, as done in [21–24] and [26-28].

The point (i) retains a central role, because it explains the need of 2D elements representing the fibre phase with nodes at mid-plane of the plies. This make possible to measure, by using the strain in the 3D elements, the separation of these mid-plane and to apply a CZM to model the toughness related to interlaminar fracture process without using zero-thickness finite elements, as explained in section3.2.

2.4 Effective algorithm for a bi-phasic decomposition

The development of a robust algorithm to identify the stiffness contributions attributed to the idealized fibre and matrix phases is one of the basic ingredients of the approach. The simplest way to perform this decomposition is based on the use of the bare fibre modulus $E^{f\text{-}bare}$ to evaluate the effective fibre modulus, $E^{f\text{-}eff}$, in Eq. 2. However, the subtraction prescribed in Eq. 3 of the fibre stiffness contribution based on $E^{f\text{-}bare}$ often leads to negative terms in the idealized matrix phase or to a non-physically admissible stiffness matrix, as shown in [24]. Indeed, the effective contribution of fibre to the overall stiffness in reinforcement direction is lower than the one that can be found by using a rule of mixture, but it is much higher than the matrix one. Therefore, a relative small overestimation of fibre contribution has noticeable with undesired effects on the properties of the idealized matrix phase obtained by subtraction.

Moreover, this strategy is not consistent with the definition of the fibre phase, given in Eq. 1 and discussed in section 2.2. Due to the fact that fibre phase represents the continuity of fibres and matrix phase the remaining properties of the whole composite, a more appropriate strategy is developed focusing on the properties of the matrix, which is an effective continuum medium with properties similar to those of the composite in the transversal direction of fibres, where they are not continuous. Hence, it

can be proposed that the Poisson's ratio of the matrix alone should be close ν_{12}^{C}, which characterize the contraction in direction 2 (transversal to fibres) for a load applied in fibre direction. Indeed, in unidirectional long fibre reinforced composites, Poisson ratios ν_{21}^{C} and ν_{12}^{C} are completely different, due the effect of fibre continuity in 1-direction: ν_{21}^{C} is much lower than ν_{12}^{C}, which is typically in the range ν_0 = 0.25-0.35 [58].

Following these observations, a new and effective strategy is devised based on the control of Poisson's ratio of matrix phase, with two main objectives:

- define a fibre phase representative of fibre continuity, with a modulus not excessively lower than $E^{f\text{-}bare}$;
- define a matrix phase positively definite with properties close to the one of the composite in the direction transversal to fibre, with a Poisson's ratio imposed to a value in the typical range of ν_{12}^{C} for unidirectional composites.

A decomposition algorithm based on the definition of matrix phase Poisson's ratio was first applied in [24] both to unidirectional and fabric plies, considering in-plane stress states, and was shown to be effective for many types of composite materials, including fabrics. It is now formulated for general three-dimensional stress states, for unidirectional plies.

To develop the algorithm, the individual terms of the stiffness matrix D^m are expressed as a function of the engineering constants of the material equivalent to the idealized matrix phase. For a three-dimensional stress state, the expressions can be found in [59]. By applying the definition of fibre and matrix phase given in Eq. 2 and the subtraction prescribed in Eq. 3, the following form is obtained:

$$\begin{cases} D_{11}^m = D_{11}^c - V_1^f E_1^{f-eff} = E_{11}^m(1-\nu_{23}^m\nu_{32}^m)Y \\ D_{22}^m = D_{22}^c - = E_{22}^m(1-\nu_{13}^m\nu_{31}^m)Y \\ D_{33}^m = D_{33}^c = E_{33}^m(1-\nu_{12}^m\nu_{21}^m)Y \\ D_{12}^m = D_{12}^c = E_{11}^m(\nu_{21}^m+\nu_{23}^m\nu_{31}^m)Y = E_{22}^m(\nu_{12}^m+\nu_{13}^m\nu_{32}^m)Y \\ D_{23}^m = D_{23}^c = E_{22}^m(\nu_{32}^m+\nu_{12}^m\nu_{31}^m)Y = E_{33}^m(\nu_{23}^m+\nu_{21}^m\nu_{13}^m)Y \\ D_{13}^m = D_{13}^c = E_{11}^m(\nu_{31}^m+\nu_{21}^m\nu_{32}^m)Y = E_{33}^m(\nu_{13}^m+\nu_{12}^m\nu_{23}^m)Y \\ D_{44}^m = D_{44}^c = G_{12}^m \\ D_{55}^m = D_{55}^c = G_{23}^m \\ D_{66}^m = D_{66}^c = G_{13}^m \end{cases} \qquad \text{Eq. 4}$$

$$Y = \frac{1}{1-\nu_{12}^m\nu_{21}^m-\nu_{23}^m\nu_{32}^m-\nu_{13}^m\nu_{31}^m-2\nu_{21}^m\nu_{32}^m\nu_{13}^m}$$

For a UD ply, the hypothesis of transverse isotropy can be conveniently introduced, so that the properties of the laminate, and consequently the properties of the matrix, are the same in the 2- and 3-directions. Therefore, some selected relations of Eq. 4 can be re-written as reported in Eq. 5:

$$\begin{cases} D_{11}^c - V_1^f E_1^{f-eff} = E_{11}^m(1-(\nu_{32}^m)^2)Y \\ D_{22}^c = E_{22}^m\left(1-(\nu_{21}^m)^2\frac{E_{11}^m}{E_{22}^m}\right)Y \\ D_{12}^c = E_{11}^m(\nu_{21}^m+\nu_{23}^m\nu_{21}^m)Y \\ D_{23}^c = E_{22}^m\left(\nu_{23}^m+(\nu_{21}^m)^2\frac{E_{11}^m}{E_{22}^m}\right)Y \end{cases} \qquad \text{Eq. 5}$$

Considering the relations between Poisson ratios derived from the matrix stiffness symmetry, Eq. 5 defines a decomposition problem where E_{11}^m, E_{22}^m, ν_{23}^m, ν_{21}^m, and $E_1^{f\text{-}eff}$ are the unknown variables. The application of a decomposition strategy based on the effects of fibre continuity on the Poisson ratio leads to solve such problem by imposing $\nu_{21}^m = \nu_0$. The resulting non-linear system is solved by using the simplex method based on the Nelder-Mead algorithm [60], implemented in the Matlab® toolbox.

Different types of UD plies are considered, and the three-dimensional decomposition problems have been solved for different values of ν_0, in the range $\nu_0 = 0.10 \div 0.40$. Table 1 reports the results obtained by using $\nu_0 = 0.3$ for three types of materials. The chosen value of ν_0 leads to obtain a physically admissible idealized matrix phase with equal E_{11}^m and E_{22}^m.

Table 1 – Application of the decomposition algorithm with $\nu_0 = 0.3$

Material	**T300-934 [39]**	**Hexcel Graphite 913C [37]**	**UD glass-fiber/epoxy [39]**
V_1^f, V_2^f (-)	0.6, 0.0	0.555, 0.0	0.5, 0.0
E_{11}^c (MPa)	148000	131000	41700
E_{22}^c (MPa)	9650	8900	13000
E_{33}^c (MPa)	9650	8900	13000
ν_{12}^c (-)	0.3	0.3	0.3
ν_{13}^c (-)	0.3	0.3	0.3
ν_{23}^c (-)	0.3	0.3	0.3
G_{12}^c (MPa)	4550	5370	3400
G_{13}^c (MPa)	4550	5370	3400
G_{23}^c (MPa)	3712	3423	3400
$E^{f\text{-}eff}$ (MPa)	231944	221354	72400
$E^{f\text{-}eff}/E^{f\text{-}bare}$ (-)	1.01	0.98	0.82
E_{11}^m (MPa)	8833	8149	12172
E_{22}^m (MPa)	8833	8149	12172
E_{33}^m (MPa)	8833	8149	12172

As evident, the obtained value of $E^{f\text{-}eff}$ results equal to 80% of the corresponding bare fibre modulus for the glass reinforced material and more than 95% for the carbon-reinforced materials. The idealized matrix phase is always a physically admissible material. The results obtained with the new decomposition strategy fulfil the objectives of the decomposition and confirm the ones obtained in [24] for the plane stress states.

3. Structure of the constitutive law for the idealized matrix phase

The sketch reported in Fig. 3 is representative of the 3D elements used in the bi-phasic model to represent the matrix phase. Matrix 3D elements connect the layers of 2D elements, which model the

idealized fibre phases of two adjacent plies, and occupy the volume between their mid-planes. Each matrix element has to be considered ideally divided into two parts, which represent half of the matrix phases referred to the upper ply and to the lower ply, respectively. Therefore, the response of the 3D element has to be a combination of the response of these two matrix semi-phases, which will be characterized by properties denoted by superscripts U and L. If t^U and t^L are the total thickness of the upper and lower plies, and the t is the thickness of the matrix element, the upper matrix semi-phase is characterized by a thickness ratio equal to $\alpha^U = t^U/2t$ and an orientation angle of θ^U, the angle depends on the material axis orientation in the upper ply. Likewise, the lower phase has a thickness ratio of $\alpha^L = t^L/2t$ and an orientation of θ^L.

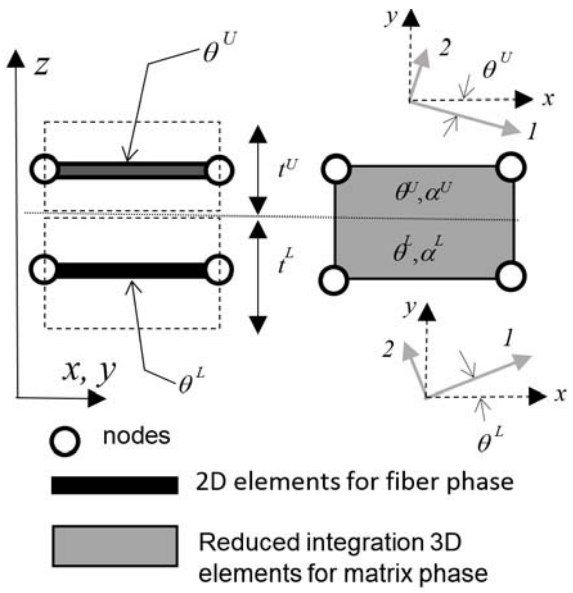

Fig. 3 – Structure and reference systems related to a 3D element for the idealized matrix phase

The constitutive law for the matrix element is formulated in a reference frame attributed to the matrix element, characterized by axes *x, y, z*, where the *z* axis is along the normal of the laminate. However, the law is actually a combination of the responses of the two semi-phases, which are described in the material axes of the adjacent plies, with indices 1, 2, 3. The material axis 3 and the element axis *z* are

coincident. The next sub-sections describe the main aspects of the constitutive law attributed to the idealized matrix phase.

3.1 Equivalent properties in the out-of-plane direction

The out-of-plane stress components carried by the matrix phase σ_{zz}^{m}, τ_{xz}^{m}, and τ_{yz}^{m}, are transmitted through the interfaces of the plies. According to simple equilibrium considerations, it is reasonable to assume that such stress components are identical in the two semi-phases represented in the 3D element. Consequently, the distribution of out-of-plane strains in the semi-phases depends on the local material properties. The overall normal strain ε_{zz}^{m} in the element is written as a weighted sum of the strains in the two matrix semi-phases, as expressed in Eq. 6.

$$\varepsilon_{zz} = \alpha^{U}\varepsilon_{33}^{U} + \alpha^{L}\varepsilon_{33}^{L} \qquad \text{Eq. 6}$$

The normal out-of-plane strains in each one of the two semi-phases, $\varepsilon_{33}^{U,L}$, are expressed in Eq. 7 taking into account the coupling between the normal stress-strain components.

$$\varepsilon_{33}^{U,L} = \frac{1}{E_{33}^{U,L}}\sigma_{33}^{U,L} - \frac{\nu_{13}^{U,L}}{E_{11}^{U,L}}\sigma_{11}^{U,L} - \frac{\nu_{23}^{U,L}}{E_{22}^{U,L}}\sigma_{22}^{U,L} \qquad \text{Eq. 7}$$

The following relation is obtained by combining Eq. 6 and Eq. 7 and by considering $\sigma_{zz}^{m} = \sigma_{33}^{U} = \sigma_{33}^{L}$:

$$\varepsilon_{zz} = \left(\frac{\alpha^{U}}{E_{33}^{U}} + \frac{\alpha^{L}}{E_{33}^{L}}\right)\sigma_{zz}^{m} - \alpha^{U}\left(\frac{\nu_{13}^{U}}{E_{11}^{U}}\sigma_{11}^{U} + \frac{\nu_{23}^{U}}{E_{22}^{U}}\sigma_{22}^{U}\right) - \alpha^{D}\left(\frac{\nu_{13}^{L}}{E_{11}^{L}}\sigma_{11}^{D} + \frac{\nu_{23}^{L}}{E_{22}^{L}}\sigma_{22}^{L}\right) \qquad \text{Eq. 8}$$

The solution of Eq. 8 for σ_{zz}^{m} is provided in Eq. 9. It can be observed that σ_{zz}^{m} can be evaluated once that an equivalent out-of-plane stiffness modulus is defined, and the in-plane stress components are known. The expression of the equivalent modulus is given in Eq. 10.

$$\sigma_{zz} = \left(\frac{E_{33}^{U}E_{33}^{L}}{\alpha^{U}E_{33}^{L}+\alpha^{L}E_{33}^{U}}\right)\left[\varepsilon_{zz} + \alpha^{U}\left(\frac{\nu_{13}^{U}}{E_{11}^{U}}\sigma_{11}^{U} + \frac{\nu_{23}^{U}}{E_{22}^{U}}\sigma_{22}^{U}\right) + \alpha^{L}\left(\frac{\nu_{13}^{L}}{E_{11}^{L}}\sigma_{11}^{L} + \frac{\nu_{23}^{L}}{E_{22}^{L}}\sigma_{22}^{L}\right)\right] \quad \text{Eq. 9}$$

$$E_{zz}^{eq} = \frac{E_{33}^{U}E_{33}^{L}}{\alpha^{U}E_{33}^{L}+\alpha^{L}E_{33}^{U}} \quad \text{Eq. 10}$$

For the out-of-plane shear stress components, similar results are obtained. Eventually, two equivalent out-of-plane shear stiffness moduli are defined as in Eq. 11.

$$\begin{cases} G_{yz}^{eq} = \frac{G_{23}^{U}G_{23}^{L}}{\alpha^{U}G_{23}^{L}+\alpha^{L}G_{23}^{U}} \\ G_{xz}^{eq} = \frac{G_{13}^{U}G_{13}^{L}}{\alpha^{U}G_{13}^{L}+\alpha^{L}G_{13}^{U}} \end{cases} \quad \text{Eq. 11}$$

Taking into account the previous results, the out-of-plane stress state in the matrix element is evaluated through the relations reported in Eq. 12.

$$\begin{cases} \sigma_{zz}^{m} = E_{zz}^{eq}\left[\varepsilon_{zz} + \alpha^{U}\left(\frac{\nu_{13}^{U}}{E_{11}^{U}}\sigma_{11}^{U} + \frac{\nu_{23}^{U}}{E_{22}^{U}}\sigma_{22}^{U}\right) + \alpha^{DW}\left(\frac{\nu_{13}^{L}}{E_{11}^{L}}\sigma_{11}^{L} + \frac{\nu_{23}^{L}}{E_{22}^{L}}\sigma_{22}^{L}\right)\right] \\ \tau_{xz}^{m} = G_{xz}^{eq}\gamma_{xz} \\ \tau_{yz}^{m} = G_{yz}^{eq}\gamma_{yz} \end{cases} \quad \text{Eq. 12}$$

3.2 Introduction of an interlaminar cohesive zone model

The procedure described in [35,36] for the introduction of a CZM in finite thickness elements with a single integration point is hereby applied to the matrix elements. The procedure relies on the possibility to describe the fracture process through the displacements of the mid-planes of two adjacent laminates, as shown in Fig. 1. This vector of relative displacement, $\boldsymbol{\Delta}$, is defined in Eq. 13, where it is linked to the average out-of-plane strain state between the mid-planes.

$$\Delta = \begin{Bmatrix} \Delta_{I} \\ \Delta_{II} \\ \Delta_{III} \end{Bmatrix} = \begin{Bmatrix} U_{z}^{U} - U_{z}^{L} \\ U_{x}^{U} - U_{x}^{L} \\ U_{y}^{U} - U_{y}^{L} \end{Bmatrix} = \begin{Bmatrix} \varepsilon_{zz} \\ \gamma_{xz} \\ \gamma_{yz} \end{Bmatrix} t \quad \text{Eq. 13}$$

Thanks to the link expressed in Eq. 13, a stress-strain response with damage can be defined to model the separation of the mid-plane of the plies, by including a CZM in the finite thickness elements. In this paper, the model presented in [31] is selected as a guideline to develop a constitutive response capable of representing mixed-mode delamination.

In the model implemented, the assumption of equivalent properties for mode II and mode III propagation is introduced. The out-of-plane strain components are used to define the equivalent strain components, ε_I and ε_{II}, reported in Eq. 14. Two corresponding equivalent stresses are introduced in Eq. 14 as well. If solid elements with a reduced integration scheme are adopted, the out-of-plane stress state at the single integration point is actually a representation of the average stress between the plies. Therefore, delamination is represented by the degradation of the equivalent moduli defined in Eq. 10 and in Eq. 11, as indicated in Eq. 14.

$$\begin{aligned}
&\varepsilon_I = \begin{cases} 0 & if \quad \varepsilon_{zz} \leq 0 \\ \varepsilon_{zz} & if \quad \varepsilon_{zz} > 0 \end{cases} \\
&\varepsilon_{II} = \sqrt{\gamma_{yz}^2 + \gamma_{xz}^2} \\
&\sigma_I = E_{zz}^{eq}(1 - d_{mo})\varepsilon_I \\
&\sigma_{II} = G_{xz}^{eq}(1 - d_{mo})\varepsilon_{II} = G_{yz}^{eq}(1 - d_{mo})\varepsilon_{II}
\end{aligned} \qquad \text{Eq. 14}$$

The scalar variable d_{mo} represents the loss of transmission capability of the out-of-plane stress components between the plies in the matrix idealized phase. The introduction of the CZM leads to the evaluation of the damage d_{mo}, driven by the equivalent strain components. The damage evolution is shaped so as to introduce a bilinear response in the σ_I-ε_I and σ_{II}-ε_{II}. The damage threshold is set at the strength values σ_{I0} and σ_{II0} (see Fig. 1). The final strain ε_{IF} and ε_{IIF} are identified by imposing that the energy required to reach d_{mo} = 1 matches the critical energy release rates G_{Ic} and G_{IIc}, according to Eq. 15:

$$\begin{aligned}
&G_{Ic} = \int_0^{\Delta_{If}} \sigma_I d\Delta_I = t \int_0^{\varepsilon_{If}} \sigma_I d\varepsilon_I \\
&G_{IIc} = \int_0^{\Delta_{IIf}} \sigma_{II} d\Delta_{II} = t \int_0^{\varepsilon_{IIf}} \sigma_{II} d\varepsilon_{II}
\end{aligned} \qquad \text{Eq. 15}$$

Delamination occurring in a mixed mode was modelled by introducing in the damage algorithm a quadratic strength criterion and a B-K toughness criterion [61], as shown in Eq. 16, with the η exponent set equal to 1.45.

$$\left(\frac{\sigma_I}{\sigma_{I0}}\right)^2 + \left(\frac{\sigma_{II}}{\sigma_{II0}}\right)^2 = 1$$
$$G_I + G_{II} = G_{Ic} + (G_{IIc} - G_{Ic})\left(\frac{G_{II}}{G_I+G_{II}}\right)^{\eta} \quad \text{Eq. 16}$$

It can be observed that, in the developed approach, the interlaminar crack at the interface is smeared in the volume of the solid element representing the idealized matrix phase. The approach, based on CDM, requires a parameter representing a characteristic length of the element, which must be introduced to regularize the damage law, as highlighted in [15,35]. In the presented formulation, regularization was achieved by introducing the element of total thickness, t, which is necessary in order to define the stress vs. strain response according to Eq. 15. It can be observed that G_{Ic}/t must be equal to area under the stress vs. strain response, which, in a bilinear response, is given by $1/2\sigma_{I0}\varepsilon_{IF}$, so that $\varepsilon_{IF}=2G_{Ic}/(\sigma_{I0}t)$. The condition $\varepsilon_{IF} < \varepsilon_{I0}$ cannot be accepted, since in this case the energy accumulated in the element in the elastic range would exceed the one required to damage the interface. This leads to conditions on the admissible values of G_{Ic}, σ_{I0}, and t. Such conditions are typically satisfied for models laminates made of carbon- or glass-reinforced polymer matrix UD and fabric plies, as confirmed by the applications presented in [30, 31, 36-39].

3.3 Modelling of in-plane stress state and transverse cracking

For the intralaminar stress state, the assumption introduced is that the two matrix semi-phases in the element share the same strain state, so that $\varepsilon_{xx} = \varepsilon_{xx}^U = \varepsilon_{xx}^L$, $\varepsilon_{yy} = \varepsilon_{yy}^U = \varepsilon_{yy}^L$, and $\gamma_{xy} = \gamma_{xy}^U = \gamma_{xy}^L$. The strain components can be rotated in the material reference frame for each semi-phase, considering orientation angles θ^U and θ^L, so as to evaluate the in-plane stress, which are different for each semi-phase. Within the theoretical frame of a CDM approach the generic in-plane constitutive law reads

$$\begin{cases} \sigma_{11}^{U,L} = \mathrm{D'}_{11}^{U,L}\varepsilon_{11}^{U,L} + \mathrm{D'}_{12}^{U,L}\varepsilon_{22}^{U,L} + \mathrm{D'}_{13}^{U,L}\varepsilon_{33}^{U,L} \\ \sigma_{22}^{U,L} = \mathrm{D'}_{21}^{U,L}\varepsilon_{11}^{U,L} + \mathrm{D'}_{22}^{U,L}\varepsilon_{22}^{U,L} + \mathrm{D'}_{23}^{U,L}\varepsilon_{33}^{U,L} \\ \tau_{12}^{U,DL} = \mathrm{D'}_{44}^{U,L}\gamma_{12}^{U,L} \end{cases} \quad \text{Eq. 17}$$

where the apices applied at the matrix stiffness terms $D_{ij}^{U,L}$ indicate that they could be degraded according to a generic damage law, as in [62]. The stress evaluated through Eq. 17 is rotated back to the element reference frame and the overall in-plane stress contribution components in the matrix element are assembled by applying a modified rule of mixtures.

In the applications presented in this paper, a very simple damage law is implemented for the intralaminar matrix damage, with the specific objective to model a transverse matrix cracking in cross-ply laminates. In the law adopted, an intralaminar damage variable, driven by the transverse strain $\varepsilon_{22}^{U,L}$ is defined according to the expression given in Eq. 18.

$$d_{mc}^{U,L} = \begin{cases} 0 & if \quad \varepsilon_{22}^{U,L} < \varepsilon_{mc0}^{U,L} \\ 1 + \frac{\sigma_{mc0}^{U,L}}{E_{22}^{U,L}\left(\varepsilon_{mcf}^{U,L} - \varepsilon_{mc0}^{U,L}\right)} - \frac{1}{E_{22}^{U,L}\varepsilon_{22}^{U,L}}\left(\frac{\sigma_{mc0}^{U,L}\varepsilon_{mc0}^{U,L}}{\varepsilon_{mcf}^{U,L} - \varepsilon_{mc0}^{U,L}} + \sigma_{mc0}^{U,L}\right) & if \quad \varepsilon_{mc0}^{U,L} \le \varepsilon_{22}^{U,L} < \varepsilon_{mcf}^{U,L} \\ 1 & if \quad \varepsilon_{22}^{U,L} \ge \varepsilon_{mcf}^{U,L} \end{cases} \quad \text{Eq. 18}$$

where $\varepsilon_{mc0}^{U,L}$ is the strain at damage threshold, $\sigma_{mc0}^{U,L} = E_{22}^{U,L}\varepsilon_{mc0}^{U,L}$ is the strength of the matrix phase in transverse direction, and $\varepsilon_{mcf}^{U,L}$ is the strain at unit damage. The damage evolution law is shaped to obtain a triangular σ_{22} - ε_{22} response, analogous to the response introduced in CZM for delamination. The damage law can be adopted to represent the development of a single transverse matrix crack in the element, as shown in Section 5. The material parameter $\varepsilon_{mcf}^{U,L}$ represents the strain corresponding to a unit damage, so that the area below the triangular stress vs. strain response is $1/2\sigma_{mc0}^{U,L}\varepsilon_{mcf}^{U,L}$. This area should be set equal to the energy per unit volume required to completely open a transverse crack in the volume occupied by the matrix element. If the critical energy release rate for the development of a transverse crack, $G_{mcc}^{U,L}$, is known, the response is calibrated by setting:

$$\varepsilon_{mcf}^{U,L} = \frac{2G_{mcc}^{U,L}}{\sigma_{mc0}^{U,L} l_{el}} \quad \text{Eq. 19}$$

where l^{el} is the characteristic length of the element, required to regularize the law, since $G_{mcc}^{U,L}$ is the critical energy release rate per unit surface. Actually, the strength attributed to the matrix has to be calibrated considering the in-situ strength of the of the group of plies with a homogeneous orientation where the transverse crack can develop. Such strength can be related to $G_{mcc}^{U,L}$ through the theory developed in [63] and also applied in [52], which leads to Eq. 20:

$$\sigma_{mc0}^{U,L} = \sqrt{\frac{8G_{mcc}^{U,L}}{\pi T^{U,L} \Lambda_{22} \xi}} \quad \text{Eq. 20}$$

where $T^{U,L}$ is the overall thickness of the group of plies with a homogeneous orientation. The parameter ξ can be set equal to unit value [52], and Λ_{22} is a function of the properties of composite material, as indicated in Eq. 21.

$$\Lambda_{22} = 2\left(\frac{1}{E_{22}} - \frac{\nu_{12}^2}{E_{11}}\right) \quad \text{Eq. 21}$$

The damage variable $d_{mc}{}^{U,L}$ degrades the stiffness modulus $E_{22}{}^{U,L}$ and also the Poisson ratios $\nu_{21}{}^{U,L}$ and $\nu_{23}{}^{U,L}$. After the evaluation of the damage variable, the engineering constants were degraded and then used to build the damaged terms of the stiffness matrix expressed in Eq. 17, for both semi-phases represented by the 3D element.

3.4 Combination of stress states in 3D elements

The final combination of stress states relating to the semi-phases requires to solve some aspects that arise when an interlaminar crack develops.

Indeed, in the presence of a delamination, the out-of-plane strain ε_{zz} and the thickness of the matrix element may become very large (see Fig. 4). Nevertheless, the constitutive laws for in-plane stress

components, expressed in Eq. 17, are considered applicable, but only in the part of the volume of the 3D element occupied by the composite material, otherwise stress resultants would be overestimated.

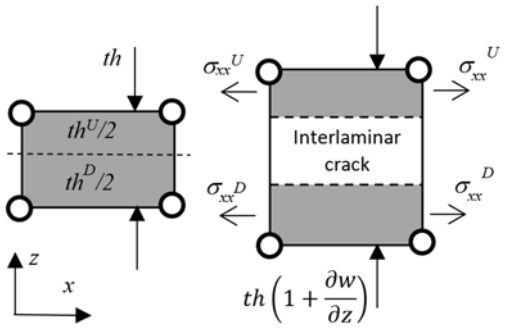

Fig. 4 – Development of mode I interlaminar crack in a matrix element

This issue can be plainly addressed by scaling down the in-plane stress components by two parameters, ω^U and ω^L, which represent the ratios between the original thickness physically occupied by the semi-phases, and the total current thickness of the deformed element, which is evaluated by knowing the component of the deformation gradient, $\boldsymbol{F}$, expressed in Eq. 22, where w represents the displacement in the z direction.

$$F_{33} = 1 + \frac{\partial w}{\partial z} \qquad \text{Eq. 22}$$

Accordingly, the expression of ω^U and ω^L are:

$$\begin{cases} \omega^U = \dfrac{t^U}{2tF_{33}} = \dfrac{\alpha^U}{F_{33}} \\ \omega^L = \dfrac{t^L}{2tF_{33}} = \dfrac{\alpha^L}{F_{33}} \end{cases} \qquad \text{Eq. 23}$$

The rule of mixture provided in Eq. 24 is used to combine the in-plane stress contributions of the matrix semi-phases, once they were rotated back to the element reference frame.

$$\begin{cases} \sigma_{xx}^{m} = \omega^{U}\sigma_{xx}^{U} + \omega^{L}\sigma_{xx}^{L} \\ \sigma_{yy}^{m} = \omega^{U}\sigma_{yy}^{U} + \omega^{L}\sigma_{yy}^{L} \\ \tau_{xy}^{m} = \omega^{U}\tau_{xy}^{U} + \omega^{L}\tau_{xy}^{L} \end{cases} \quad \text{Eq. 24}$$

The new parameters ω^{U} and ω^{L} have to be used instead of the original thickness fractions, also in Eq. 12, which is modified into Eq. 25, where the interlaminar damage parameter d_{mo} is also included.

$$\begin{cases} \sigma_{zz}^{m} = E_{zz}^{eq}(1-d_{mo})\left[\varepsilon_{zz} + \omega^{U}\left(\frac{\nu_{13}^{U}}{E_{11}^{U}}\sigma_{11}^{U} + \frac{\nu_{23}^{U}}{E_{22}^{U}}\sigma_{22}^{U}\right) + \omega^{L}\left(\frac{\nu_{13}^{L}}{E_{11}^{L}}\sigma_{11}^{L} + \frac{\nu_{23}^{L}}{E_{22}^{L}}\sigma_{22}^{L}\right)\right] \\ \tau_{xz}^{m} = G_{xz}^{eq}(1-d_{mo})\gamma_{xz} \\ \tau_{yz}^{m} = G_{yz}^{eq}(1-d_{mo})\gamma_{yz} \end{cases} \quad \text{Eq. 25}$$

Finally, it must be considered that the application of the model requires the knowledge of the strains $\varepsilon_{33}^{U,L}$ to be used in Eq. 17, where the in-plane stress in the semi-phases are computed. The combination of Eq. 7 and Eq. 25 provides the ratio between the out-of-plane strain in the semi-phases and the overall strain of the element, which is given in Eq. 26.

$$\frac{\varepsilon_{33}^{U,L}}{\varepsilon_{zz}} = \frac{\frac{1}{E_{33}^{U,D}}\sigma_{zz}^{U,L} - \frac{\nu_{13}^{U,L}}{E_{11}^{U,L}}\sigma_{11}^{U,L} - \frac{\nu_{23}^{U,L}}{E_{22}^{U,L}}\sigma_{22}^{U,L}}{\frac{1}{(1-d_{mo})E_{zz}^{eq}}\sigma_{zz} - \omega^{U}\left(\frac{\nu_{13}^{U}}{E_{11}^{U}}\sigma_{11}^{U} + \frac{\nu_{23}^{U}}{E_{22}^{U}}\sigma_{22}^{U}\right) - \omega^{L}\left(\frac{\nu_{13}^{L}}{E_{11}^{L}}\sigma_{11}^{L} + \frac{\nu_{23}^{L}}{E_{22}^{L}}\sigma_{22}^{L}\right)} \quad \text{Eq. 26}$$

A simplified form is obtained in Eq. 27.

$$\varepsilon_{33}^{U,L} = \frac{E_{zz}^{eq}(1-d_{mo})}{E_{33}^{U,L}}\varepsilon_{zz} \quad \text{Eq. 27}$$

It can be observed that, when interlaminar damage is null, Eq. 27 prescribes that the out-of-plane strains are distributed according to the ratios between the equivalent and the local out-of-plane moduli. This solution can be considered acceptable and consistent with the assumptions made to combine the out-of-plane stress states. Conversely, in the presence of interlaminar damage, the most critical issue is to avoid an unacceptable overestimation of the Poisson ratio effects due to the large values of the overall ε_{zz} strain. The application of Eq. 27 leads to reduce the local $\varepsilon_{33}^{U,L}$ strains as the interlaminar damage grows. However, this approximation maintains the capability of providing a reasonable estimation of

the in-plane stress states provided by the matrix phase even in case of a fully developed interlaminar crack, as proved in the following Section 4.

3.5 Flow chart of the constitutive law

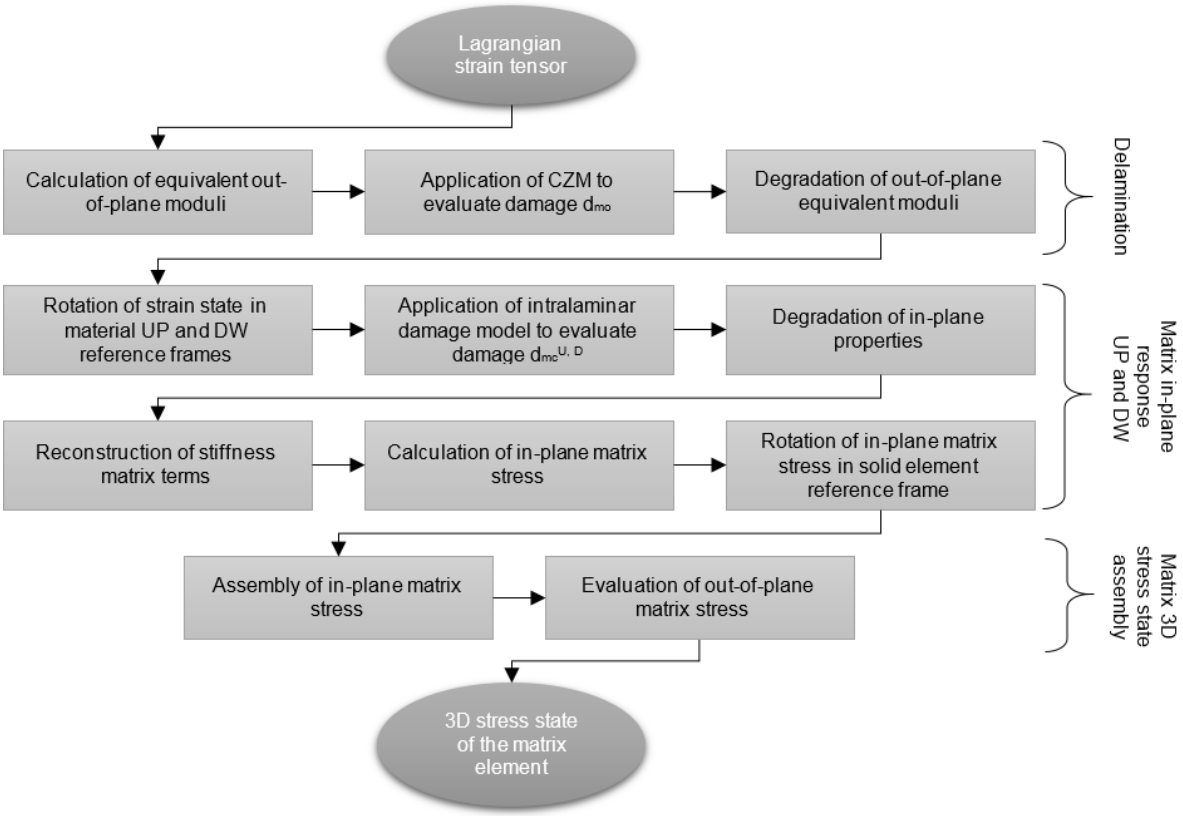

Fig. 5 – Basic structure of the constitutive law of the matrix phase

The structure of the constitutive law for the matrix can be adapted to different types of CZM and CDM to represent the onset and the evolution of matrix damage and its effects on matrix-dominated responses. The damage laws presented in the previous sub-sections are implemented in a VUMAT subroutine linked to the Abaqus/Explit code. In the subroutine, as a first step, Lagrangian strains are evaluated from the deformation gradient provided by the code and are used to calculate the interlaminar damage. Thereafter, the strain components in the material reference frame are evaluated for both semi-

phases, and the $\varepsilon_{33}^{U,L}$ are approximated through Eq. 27. Such strain state is used to evaluate through Eq. 17 the in-plane stress components for both semi-phases, by applying the chosen intralaminar damage model. In the final phase, the parameters $\omega^{U,L}$ are calculated to apply Eq. 25, providing the final out-of-plane stress components. Subsequently, the in-plane stress state of the two semi-phases are rotated in the element reference frame and assembled through Eq. 24. A simplified flow chart of the subroutine is provided in Fig. 5.

4. Modelling of delamination phenomena

4.1 Application of the bi-phasic modelling technique to DCB and ENF tests

The capability of modelling delamination by using the developed approach is assessed considering the stable development of a mode I interlaminar crack obtained in a Double Cantilever Beam (DCB) test, and the unstable propagation of a mode II interlaminar crack during an End Notched Flexure (ENF) test. Attention is focused on the possibility to accurately represent delamination between plies by using the CZM embedded in the 3D elements, still obtaining a reliable estimation of in-plane stress components during fracture process. In the models used in this activity, the in-plane response of the composite is considered linear elastic, whereas the evaluation of the interlaminar damage variable d_{mo} is based on the CZM described in sub-section 3.2, with maximum stress (σ_{I0}, σ_{II0}) and critical energy release rates (G_{Ic}, G_{IIc}) as material parameters.

The DCB and ENF tests considered for the verification were performed on 25 mm wide and 250 mm long composite specimens with a $[0]_{24}$ lay-up of Hexcel 913C-HTA graphite/epoxy unidirectional plies, with a cured ply thickness of 0.132 mm. The experimental procedure was described in detail in [44], where the in-plane properties of the material were also reported. Such properties are completed by applying transverse isotropy assumptions in order to apply the decomposition procedure described in sub-section 2.4, with results reported in Table 1. The specimens were produced with a pre-introduced

crack at the mid-plane of the laminates, obtained by the insertion of a PTFE sheet. The development of delamination from such pre-induced cracks is conveniently represented by applying the presented modelling technique only in the central region of the laminate, following the approach assessed in [36]. Therefore, only the four central plies of the $[0]_{24}$ lay-up are meshed according to the bi-phasic modelling technique, as shown in Fig. 6-A. The upper and lower sub-laminates representing the other plies of the lay-up are represented by means of laminated continuum shell elements (*SC8R* [64]). Hexahedral reduced integration elements (*C3D8R* [64]) are used for the matrix phase, whereas membrane elements (*M3D4R* [64]) are used for fibre phase. The charachteristic length of the element in *x*-*y* plane is set at 0.5 mm. A unit damage level, d_{mo}=1, was imposed at the beginning of the analysis to the matrix elements in the central row corresponding to the pre-cracked layer. Such damage does not affect the stiffness of the element for compressive normal stress, therefore the contact between the two arms of the specimens is represented in the models.

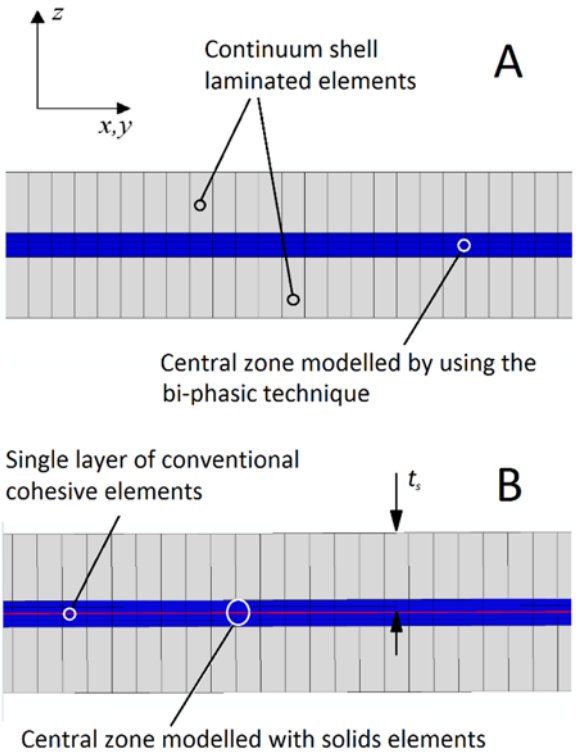

Fig. 6 – Mesh detail of DCB and ENF models: (A) bi-phasic model, (B) conventional model

All the analyses are performed by using the Simulia Abaqus/Explicit code. In the DCB model, displacements are applied by defining two rigid bodies with the set of nodes highlighted in Fig. 7-A. The reference nodes of such rigid bodies are let free to rotate about the *y* axis and to translate along the *x* axis. The velocities along the *z* direction are smoothly increased to avoid the excitement of vibrations in opposite directions for the upper and lower nodes.

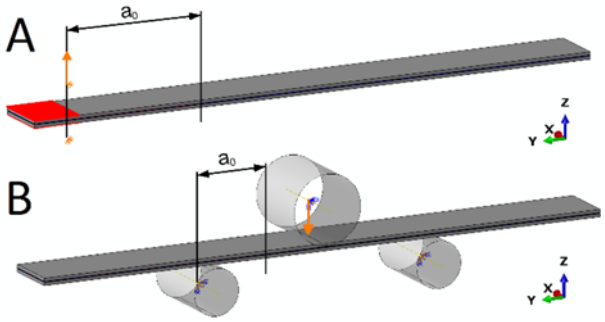

Fig. 7 – Numerical models: (A) DCB test, (B) ENF test

The ENF model is shown in Fig. 7-B, including the three rigid analytical cylindrical surfaces that were used to represent the metallic rollers adopted in order to apply the load and to support the specimen. A quasi-static analysis is performed by gradually increasing the velocity in the *z* direction of the rigid cylinder at the centre of the specimen, which is set in contact with the upper surface of the laminate. The other two lateral rigid cylinders are kept fixed and set in contact with the lower surface of the laminate.

In both models, the interlaminar properties of strength and toughness are σ_{I0}=20 MPa, σ_{II0}=50 MPa, G_{Ic}=0.24, and G_{IIc}=1.05 [44].

4.2 Numerical results and correlation with experimental data for DCB tests

The numerical-experimental correlation obtained in the analysis of the DCB test is presented in Fig. 8, where the numerical load vs. displacement curve is compared with the results obtained in five experimental tests. As prescribed by ASTM regulations [65], preliminary pre-opening phases were

conducted to achieve a more representative crack tip of a real interlaminar fracture, rather than the blunt one obtained by inserting the PTFE sheet in the lamination sequence. The slight discrepancy in the slope in the elastic range can be attributed to the difficulty to correctly identify the crack tip position at end of the pre-opening phase. The maximum force levels and the response during the crack propagation are captured with appreciable accuracy by the hybrid bi-phasic model of the specimen. For a comparison and a clarification of the techniques adopted, the same mesh is also used to apply the hybrid technique validated in [30, 31], where membrane 2D elements are characterized by considering the complete in-plane response of the plies and the hexahedral 3D elements carries only out-of-plane stress components. The force vs. displacement curve is close to that obtained by the bi-phasic model and is reported in Fig. 8.

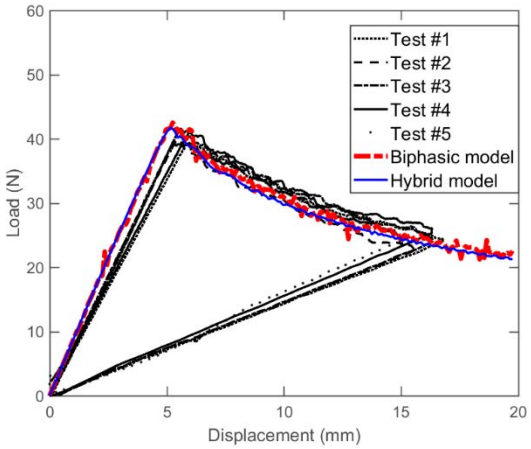

Fig. 8 – Correlation of experimental and numerical load-displacement responses of DCB for the bi-phasic model and the original hybrid technique [30, 31]

The numerical contour shown in Fig. 9-A, refers to the interlaminar damage variable d_{mo} in the crack tip zone, during the crack propagation phase. During the crack opening, each DCB arm undergoes a significant bending, such that the in-plane stress σ^{m}_{xx} in the matrix phase should increase as the elements are closer to the crack tip. Such response is correctly represented by the model, as shown in Fig. 9-B, which refers to the total σ^{m}_{xx} stress assembled from the stress states evaluated in the matrix semi-phases.

For the elements in the wake of the crack, the expected gradients both in the longitudinal and in the vertical direction are represented. Indeed, the stress σ^m_{xx} in Fig. 9-B increases along the longitudinal direction also for the elements in the central layer, where the interlaminar matrix damage develops. The in-plane stress values in such layer are identical for both matrix semi-phases and consistent with the stress levels obtained in the adjacent undamaged layers. Hence, the through-the-thickness stress gradient is captured without significant jumps. Such result represents an assessment of the approximation introduced in section 3.4 to mitigate the effects of the large ε_{zz} that develops when a mode I interlaminar crack propagates. The stress σ^m_{xx} in the elements representing the idealized matrix phase is noticeably lower than the stress σ^f_{xx}, carried by the idealized fibre phase, shown in Fig. 9-C. The sum of these two stress contributions, taken in correspondence of the same displacements, is close to the stress σ^c_{xx} presented in Fig. 9-D, which is the stress carried by the membrane elements in the analyses performed with the hybrid technique, where the 2D elements carries the whole in-plane stress state of the composites.

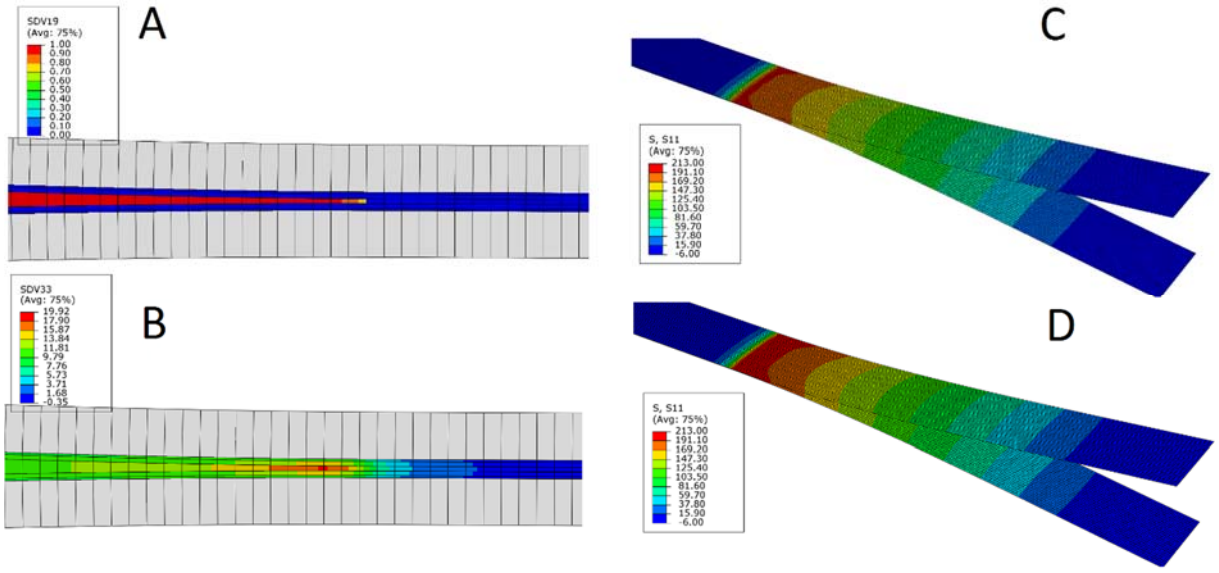

Fig. 9 – Contour in the analysis of the DCB test: (A) interlaminar damage, (B) σ^m_{xx} stress in the matrix phase, (C) σ^f_{xx} stress the membrane elements of the fibre phase, (D) total σ^c_{xx} in membrane elements with the hybrid original technique

4.3 Numerical results and correlation with experimental data for ENF tests

The correlation of load-displacement responses of five ENF tests with the one of the numerical model is presented in Fig. 10. It can be observed that the FE analysis correctly model all the quantitative aspects of the experimental curves. The load drop corresponds to the unstable propagation of the crack, which is expected considering the a_0/L of 0.5 value adopted in the test [66]. In the two contours presented in Fig. 11, the numerical crack propagation is described by reporting the distribution of interlaminar damage d_{mo} at different values of central cylinder displacement. After an initial stable development of a numerical process zone, it can be observed that damage suddenly propagates in the central layer, with a negligible increment of cylinder displacement.

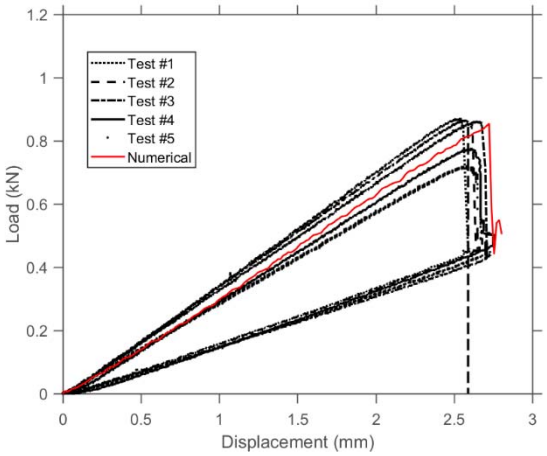

Fig. 10 – Correlation of experimental and numerical load-displacement responses of ENF

The contour reported in Fig. 12 is referred to the total in-plane σ^m_{xx} stress component in the matrix elements before the crack propagation. The tensile and compressive in-plane stress originated by the bending of the two arms in the matrix phase are correctly represented. In the central layer, the considered stress component was zero, since a pure shear strain is evaluated at the integration point of the 3D element. Accordingly, the results for the mode II delamination tests confirmed that both the propagation

of interlaminar damage and the in-plane stress evolution in the matrix phase can be correctly modelled by using the proposed approach.

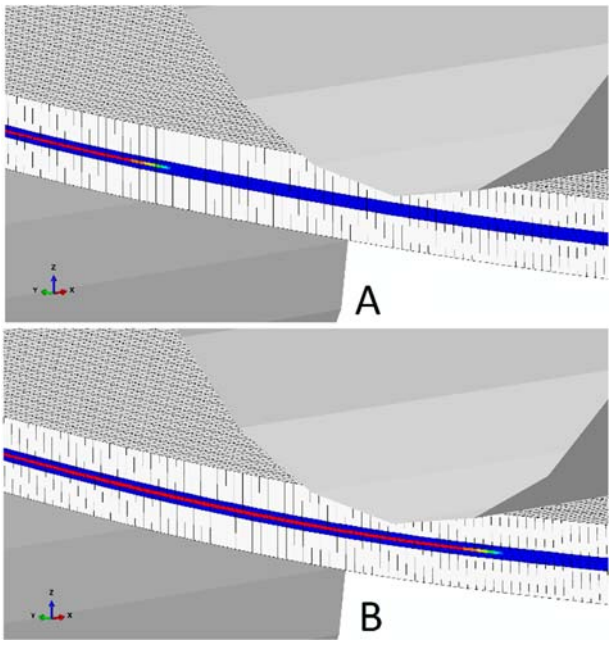

Fig. 11 – Numerical interlaminar damage in the analysis of the ENF test at different displacements of the loading cylinder: (A) at 2.63 mm, (B) at 2.70 (mm)

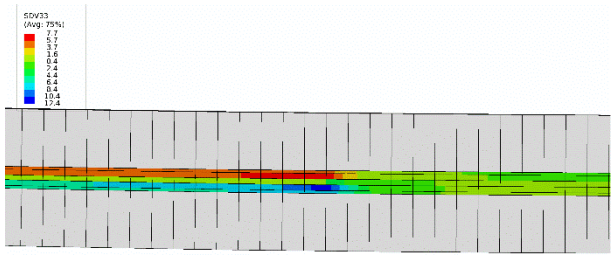

Fig. 12 – Contour of normal stress σ_{xx} in the matrix phase during the analysis of the ENF test at 1 mm of displacement

4.4 Overall considerations and comparison with a traditional cohesive approach

The presented results indicate that the CZM embedded in the matrix element is able to represent qualitative and quantitative delamination phenomena, which are modelled without using zero-thickness cohesive elements. Moreover, the analysis of the in-plane stress state evolution shows that the stress carried by the matrix phase can be reasonably predicted at the same integration points where the interlaminar damage is evaluated.

The embedment of CZM into finite thickness elements eliminates the need to introduce any penalty stiffness. Therefore, physical stiffness values are used and the stable integration time step is incremented in explicit analyses, with significant computational advantages. A comparison is carried out with a quasi-static analysis of the DCB test performed by using Simulia/Abaqus explicit code and a conventional approach based on zero-thickness cohesive elements. The conventional model is presented in Fig. 6-B: the four central plies are represented by 3D elements and a single layer of cohesive elements is introduced at the pre-cracked layer (COH3D8, [64]).

The penalty stiffness attributed to the traction-displacement response of the interface in the conventional approach, K_c, must be selected. It can be calibrated by adopting a physical point of view, where the cohesive elements are considered to represent a thin resin-rich layer [67]. Alternatively, an engineering-based approach can be used by applying Eq. 28, proposed in [34]:

$$K_c = \frac{\alpha E_{zz}}{t_s} \qquad \text{Eq. 28}$$

where E_{zz} is the physical through-thickness stiffness of the material, t_s is the physical thickness of the sub-laminates that are connected by the cohesive element, also shown in Fig. 6-B, and α is a non-dimensional parameter. A value $\alpha = 50$ was suggested in [34], for implicit analyses with a single interlaminar layer, to keep the K_c at a minimum value without undesired responses due to an excessively compliant interface in the elastic range. The initial stable time steps evaluated by the solver code for different models of the DCB tests are presented in Table 2. The stable time step also depends on the mass of the element, so that it can be artificially increased to perform quasi-static explicit analyses by using a *mass scaling* technique. However, such technique can be equivalently applied both to the conventional and the bi-phasic model, and the mass increment must be carefully calibrated, since it raises the kinetic energy in the analyses. For such reason, it is correct to compare both techniques without the adoption of mass scaling. It is clearly evident that the initial time step of the conventional model is more than one order of magnitude lower than that of the bi-phasic model. The adoption of Eq. 28 and

the attribution of additional mass to the cohesive layer, with a total mass increment of almost 14%, raise the time step in the conventional model, though it remains 40% lower than in the hybrid model #1. If all three layers were modelled, the mass increment required would be more than 50%. Moreover, the value α=50 in Eq. 28 is not adequate for models with multiple interlaminar layers to avoid large element distortions and numerical errors in quasi-static explicit analysis, which cannot be completed. On the contrary, bi-phasic models do not exhibit any convergence issue and can always be calibrated to obtain computational times significantly lower than in conventional models. These results, obtained with the bi-phasic model, are completely aligned with the ones referred to the hybrid technique presented in [36].

Table 2 – Stable time steps in explicit analyses with the bi-phasic modelling technique and conventional approaches

Model type	**Approach**	**Interfaces modelled in the central zone**	**Mass of cohesive element**	**Penalty stiffness**	**Initial stable time step (s)**	**% mass increment**
#1	Bi-phasic	All	N/A	N/A	$2.1 \cdot 10^{-8}$	0%
#2	Cohesive elements	1	0.013 mm thick resin-rich layer	0.013 mm thick resin-rich layer	$4.7 \cdot 10^{-10}$	0.18%
#3	Cohesive elements	1	0.013 mm thick resin-rich layer	Eq. 29, α=50	$7.3 \cdot 10^{-10}$	0.18%
#4	Cohesive elements	1	1 mm thick resin-rich layer	Eq. 29, α=50	$1.3 \cdot 10^{-8}$	13.8%

5. Meso-scale modelling of individual transverse matrix cracks and their density evolution

5.1 Objectives of the analyses

The constitutive law of the matrix phase is suited to model both interlaminar and intralaminar damage within the same matrix element. Different choices are possible to represent the accumulation of intralaminar matrix damage and can be implemented within the structure of the matrix constitutive law, described in Section 3. A possible choice is to represent matrix damage as a progressively accumulated diffused damage that models the stiffness degradation in the matrix-dominated responses, such as in [23,24]. However, the bi-phasic models could be adapted to a different approach, since they can also

efficiently model individual intra-laminar cracks in the matrix elements, even by using a model refined at the meso-scale level. Indeed, thanks to the specific characteristics of the approach, individual matrix cracks can be conveniently represented by using a mesh refinement equivalent to one element per ply in the through-the-thickness direction. Moreover, in the technique proposed, the stress transfer mechanisms between damaged and undamaged plies can be controlled in different ways, thus allowing a calibration of the interaction between matrix cracking and delamination. Such aspects are investigated in the activities presented in this section for cracks developing in cross-ply laminates, by applying the simplified intralaminar damage law given in Eq. 18.

5.2 Models of cross ply specimens with a statistical distribution of properties

The possibility to model individual matrix cracks is assessed by considering the evolution of crack density in cross-ply specimens, one of the cases most broadly studied in the literature regarding intralaminar matrix cracking. Several data are available in literature, such as the ones presented in [2,48,68]. In particular, the numerical analyses considered refer to a $[0/90_3/0]$ specimen made of carbon fibre reinforced UD plies, with a thickness of 0.132 mm, discussed in [48,63] and to a $[0/90_6/0]$ specimen made of glass fibre reinforced UD plies with a thickness of 0.203, presented in [2,48]. The properties and the results of the decomposition algorithm for both the materials are reported in Table 1. The bi-phasic modelling technique is applied by using 3D elements with one integration point (*C3D8R* [64]) for the matrix phase, and membrane elements (*M3D4R* [64]) for the fibre phase. The carbon fibre reinforced laminate is represented considering the structure sketched in Fig. 13-A. For the glass fibre reinforced $[0/90_6/0]$ laminate, the central block of 90° oriented plies is represented by using two membrane elements, as shown in Fig. 13-B, due to the higher number of layers.

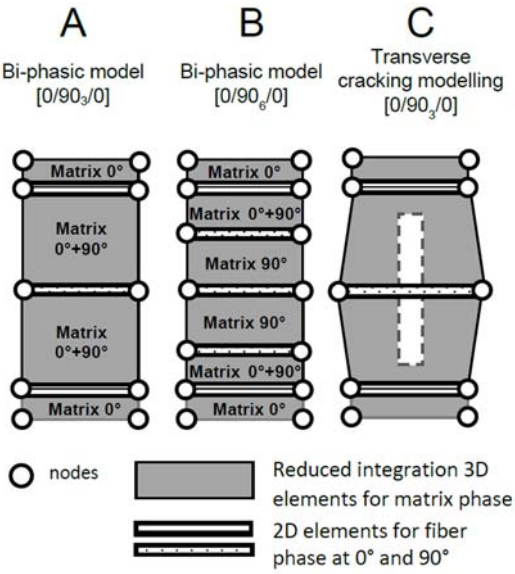

Fig. 13 – Model structure of (A) the carbon fibre reinforced, (B) the glass fibre reinforced cross-ply laminates, and (C) expected modelling mechanism of individual transverse cracks

Simplified models of the specimens are developed, which represented stripes with only one element across the width and a length of 100 mm. For the carbon fibre reinforced laminates, the three models shown in Fig. 14 are considered, with different lengths in the longitudinal direction: 0.125 mm, 0.2 mm and 0.3 mm. For the glass fibre reinforced laminate, the results presented are obtained by using a model with a typical element size of 0.2 mm. The element width is kept equal to the element length. Simulia Abaqus/Explicit code is used to simulate a quasi-static tension test. The nodes at one end of the strip are included in a rigid body, which is moved at a smoothly increasing velocity in the longitudinal direction, until an average strain of 0.01 mm/mm is achieved along the strip. A similar rigid body at the opposite end is kept fixed.

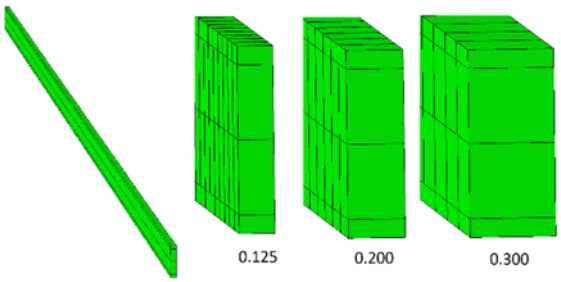

Fig. 14 – FE models of the strip of the cross-ply laminate

A damage variable, d_{mc}, evolves as prescribed in Eq. 18 and affects the Young Modulus E_{22}^{m} of the matrix semi-phase in the direction perpendicular to the fibres. Owing to the localization consequent to strain softening, the damage development may simulate the opening of a transverse matrix crack in an individual element. In particular, the deformation mechanism sketched in Fig. 13-C is predicted for the case of carbon fibre reinforced laminate, when the intralaminar damage variables are contemporarily activated in the semi-phases of two adjacent matrix elements. For the glass fibre reinforced laminate, the mechanism is similar, though the crack should also be produced in the two central matrix elements, shown in Fig. 13-B. The response of the membrane elements representing the 90° oriented fibres, set between the semi-phases, provides a null stiffness contribution in the crack opening direction. Accordingly, they should not oppose to the aforementioned deformation mechanism.

In the experimental evidence regarding the development of transverse matrix cracking in off-axis plies of cross-ply laminates, cracks appear after a certain threshold, but do not appear simultaneously. Indeed, a distinctive aspect of the phenomenon is represented by the evolution of crack density per unit length, μ. To represent the progressive development of matrix cracks, strength properties in the transverse direction must be statistically distributed [6,69]. Such aspect was taken into account in the analytical and numerical models presented in [48] and in [52], where normal distributions of strength were used.

In the models of the stripes of cross-ply laminates presented in this paper, a Weibull distribution is adopted for the strength in the elements, with the form given in Eq. 29.

$$\phi = \left(\frac{\sigma_{mc0}}{\sigma^{*}_{mc0}}\right)^{w} \qquad \text{Eq. 29}$$

where w is the shape parameter and σ^{*}_{mc0} is the scale parameter of the distribution. A procedure was developed in [69] to obtain the values of strength distribution parameters in the volume of a specimen, from the experimental evolution of the density of cracks at increasing load levels. In the present work, an initial guess for the distribution parameters of strength is found by applying such procedure to the

results reported in [48] for the transverse crack densities in the $[0/90_3/0]$ and in the $[0/90_6/0]$ laminates. Parameters are eventually adjusted to obtain a best fit with experimental data. Final values of σ^*_{mc0} = 80 MPa and w = 17 are adopted for the carbon reinforced laminate. A distribution with a scale parameter, σ^*_{mc0}, of 124 MPa and a shape parameter, w, of 5 is defined for the glass fiber reinforced laminate. A Matlab™ script is used to distribute the strength σ_{mc0} among the elements of the strip models according to the distributions identified. The semi-phases of vertically adjacent matrix elements are characterized by the same strength level. Therefore, intralaminar damage is contemporarily activated, at a given location along the longitudinal axis, for all the matrix elements in the 90° oriented blocks, as requested to activate the mechanism presented in Fig. 13-C.

5.3 Deformation and stress transfer mechanisms due to a transverse crack in the model

The development of a single crack in the strip modelled by using 0.2 mm long elements in the $[0/90_3/0]$ carbon reinforced laminate is described in Fig. 15-A and Fig. 15-B, which are referred to the contour of the longitudinal strain. In Fig. 15-A, it can be seen that the initial activation of the intralaminar damage variable in the 90° oriented semi-phases induces a strain localization. Then, the damage evolves until it reaches the unit value and leads to the condition presented in Fig. 15-B. In both figures, displacements are amplified to clearly show the deformation mechanism as well as the contraction due to the effects of the Poisson ratio in the vertical direction. The evolution of the longitudinal stress in the upper central element is presented in Fig. 15-C. The response of the element is a combination of the response of two matrix semi-phases, as explained in section 3. It can be observed that the stress in the matrix semi-phase belonging to the 90°-oriented ply, σ_{xx}^L, decreases to a null value. Indeed, the load path for longitudinal stress is interrupted in the 90°-oriented ply, due to the presence of the crack. On the contrary, the matrix semi-phase belonging to the 0°-oriented ply is undamaged. In the presence of a crack in the 90°-oriented layer, the constitutive law predicts an increment of the stress value, σ_{xx}^U, in the upper semi-phase of the element, which represents the matrix-dominated response of the undamaged

0°-oriented ply. Hence, the numerical technique is able to represent a mechanism of stress transfer between the plies, which is modelled within a single matrix element during the development of a transverse crack. The total stress in the element, $\sigma_{xx}^{TOT} = \sigma_{xx}^{U} + \sigma_{xx}^{L}$, is approximately constant.

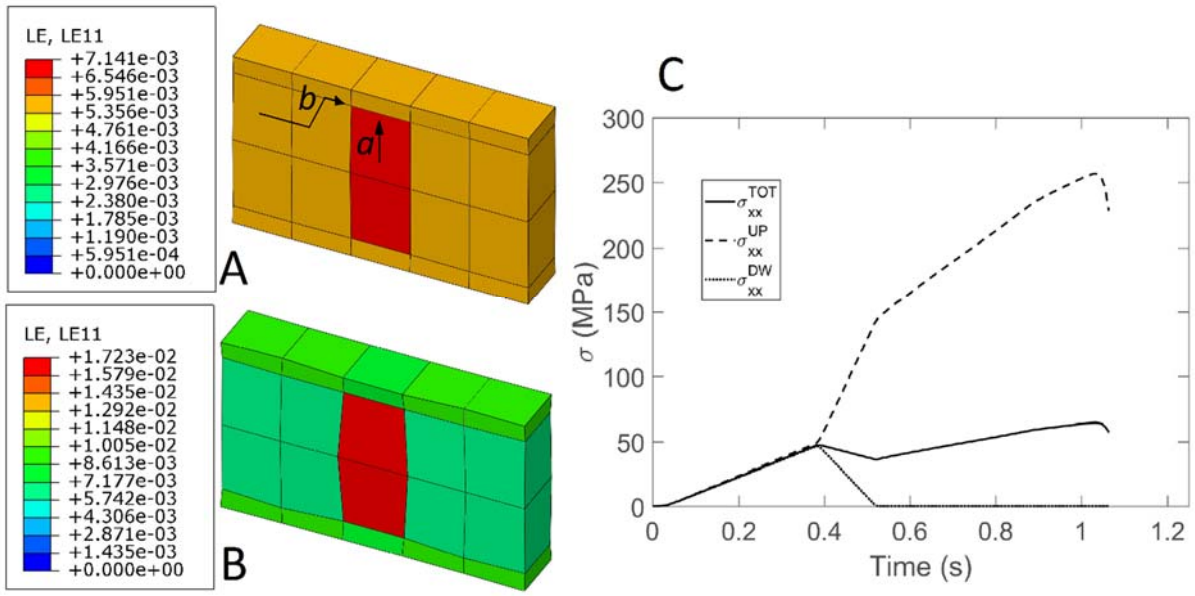

Fig. 15 – Modelling of individual crack opening: (A) strain contour at crack onset, (B) strain contour at unit damage level, (C) evolution of longitudinal stress in the semi-phases of the matrix element

The mechanism shown in Fig. 15 confirms the expected behaviour sketched in Fig. 13-C. It can be seen that, in the bi-phasic model, confinement effects due to the presence of undamaged adjacent plies do not oppose to transverse crack development. Once the crack has developed, the load path in the matrix semi-phases of the 90° oriented plies is interrupted, but the load is re-introduced in the elements of the damaged layer through two mechanisms:

a) the internal stress transfer mechanisms between the matrix semi-phases, previously discussed and represented in Fig. 15-C (load path *a* in Fig. 15-A);

b) the development of interlaminar shear stress in matrix elements close to the cracked one, in the longitudinal direction: interlaminar shear transfers the load from the 90° oriented layer, where the stress path is interrupted by the crack, to the elements of the 0° oriented layers

(load path *b* in Fig. 15-A); such second transfer mechanism will be analysed more in detail in the following sub-sections.

5.4 Numerical results for crack density evolution

The stress transfer between the plies in the numerical model allows to re-introduce the loads in the undamaged zone of the 90° oriented block. Hence, it is fundamental to determine the development of subsequent cracks in such layer, as the overall strain increases. In the numerical analyses, the progressive development of individual cracks is indeed modelled, as it is represented in the sequence of strain and damage contours shown in Fig. 16, referred to the $[0/90_3/0]$ laminate. The strain contours in Fig. 16-A indicates that new localizations progressively appear at an increasing level of average strain. Local strain also increases in the elements already damaged, to complete the crack opening. The damage contour presented in Fig. 16-B is taken at the same simulation time of the last strain contour in Fig. 16-A. It can be seen that intralaminar damage in the semi-phase completely evolved in the oldest cracks and it progressively increasing in the more recent ones.

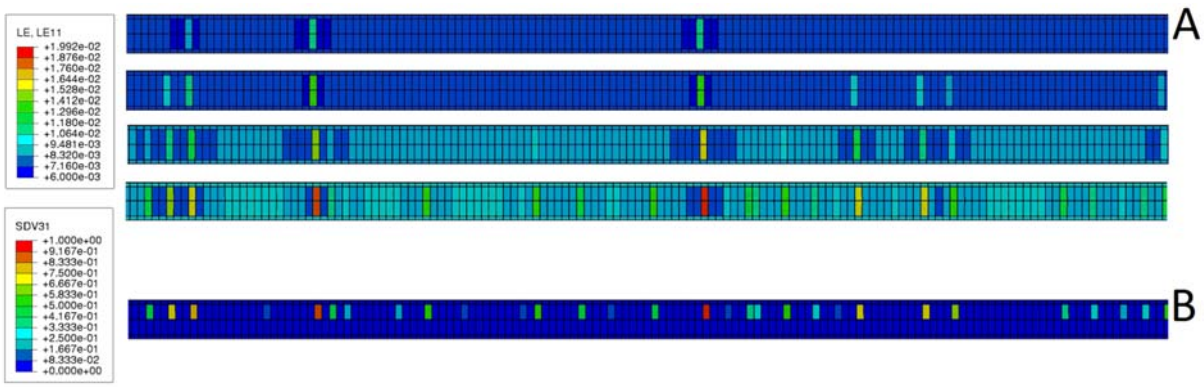

Fig. 16 – (A) numerical evolution of longitudinal strain localizations due to the intralaminar damage and (B) contour of intralaminar damage in the lower matrix semi-phase

A post-processing technique is applied to evaluate the density of cracks in the numerical solutions at various steps. A Python script is used to extract automatically, from the solver output database, the elements along a longitudinal strip with activated intralaminar damage ($d_{mc} > 0$). The number of these elements corresponds to the number of cracks and gives the crack density at each step, which correspond

to an average stress level applied to laminate. Numerical densities are then plotted against the average stress levels and compared with experimental plots of density evolution.

The numerical curves of density evolution for the different mesh sizes in the model of the carbon reinforced laminate are correlated with the experimental data in Fig. 17. Correlation is generally acceptable, despite some discrepancies in the initial phases of crack development. However, the slope of the density vs. average stress curve is well captured. It can be observed that the best solution is obtained by using the smallest mesh size. The development of individual matrix cracks is well captured up to a density level higher than a crack per millimetre, without exhibiting over-constraining effects due to the adjacent plies. Crack evolution depends on the statistical distribution of properties and the sensitivity of the results to the mesh size in the longitudinal direction is quite limited, thanks to damage law regularization based on the characteristic length of the element (Eq. 19).

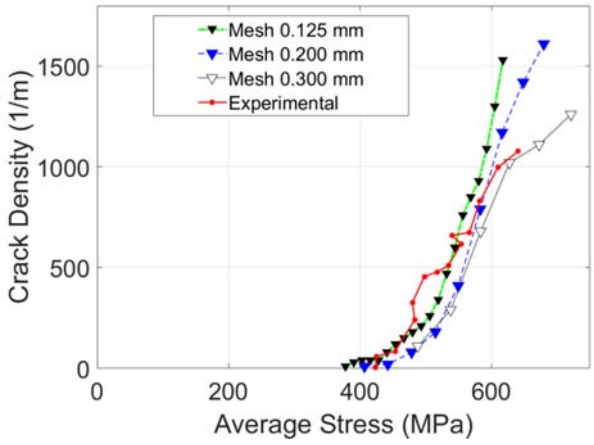

Fig. 17 – Numerical-experimental correlation of crack density evolution in a carbon reinforced cross-ply laminate, for different mesh sizes

5.5 Crack density evolution in the presence of interactions between transverse cracking and delamination

The results presented confirm that, for the $[0/90_3/0]$ carbon fibre reinforced laminate, the effects of potential delaminations are not needed to be modelled in order to achieve a good numerical-experimental correlation, as stated in [48]. However, this is not expected to be true for the $[0/90_6/0]$ glass fibre

reinforced laminate. In this second case, the crack density evolution was characterized by a progressive reduction of the slope in the curve of density vs. average state, beyond a certain threshold [2,48]. Such phenomenon was attributed to the onset of delamination processes between the 0° and the 90° oriented plies: delamination interfered with the load transfer mechanisms between the plies and opposed any further development of the cracking in the 90° oriented plies. Therefore, such case represents an important benchmark for the bi-phasic modelling technique in order to model the interaction between the two damage processes with a relatively coarse model. The interlaminar CZM for delamination is calibrated considering a uniform shear strength σ_{I0} =40 MPa, which was the expectation value of the normal distribution adopted in [48]. The other material parameters for the interlaminar damage model are expected to play a less significant role in the interaction between transverse cracking and delamination. Hence, they are kept equal to the values identified for carbon/epoxy plies considered in section 4: σ_{I0} = 20 MPa, G_{Ic} = 0.24, and G_{IIc} = 1.05. The interlaminar damage model is activated in the matrix elements between 90° oriented and 0° oriented plies, but is inhibited in the central matrix elements.

The initial results obtained in the numerical analysis, in terms of crack density evolution vs. average applied stress, are presented and compared with experimental data of [2,48] in Fig. 18-A. It can be observed that the numerical results match the experimental data up to a density of 400 cracks per meters, but do not represent the change of slope attributed to delamination phenomena. The analysis of the results is focused on the transverse shear stress that develops in the matrix elements between the 0° and the 90° oriented plies. Transverse shear is the second of the load transfer mechanisms between the plies, previously discussed in Section 5.3. According to the contour shown in Fig. 18-B, interlaminar shear stresses arise in the analysis, but they are not sufficient to promote delamination.

However, the bi-phasic approach allows to control the interaction between a transverse crack and delamination by acting on the stress transfer mechanism internal to the matrix element, based on load path *a* indicated in Fig. 15-A. Indeed, part of the stress originally carried by the 90°-oriented matrix is

internally transferred to the matrix phase of the 0°-oriented plies, within the same matrix element. It is possible to control and attenuate such mechanism by introducing a parameter, *h*, that couples the intralaminar damages of the two matrix semi-phases. The introduction of the coupling between normal stress components leads to re-formulate Eq. 24 in the following way:

$$\begin{cases} \sigma_{xx}^{m} = (1 - h d_{mc}^{L})\omega^{U}\sigma_{xx}^{U} + (1 - h d_{mc}^{U})\omega^{L}\sigma_{xx}^{L} \\ \sigma_{yy}^{m} = (1 - h d_{mc}^{L})\omega^{U}\sigma_{yy}^{U} + (1 - h d_{mc}^{U})\omega^{L}\sigma_{yy}^{L} \\ \tau_{xy}^{m} = \omega^{U}\tau_{xy}^{U} + \omega^{L}\tau_{xy}^{L} \end{cases} \quad \text{Eq. 30}$$

where d^{U}_{mc} and d^{L}_{mc} are the intralaminar damage parameters in the upper and lower semi-phases, respectively. The coupling parameter *h* roughly models, at the meso-scale level, phenomena that would require a much more refined mesh to be correctly represented in a finite element analysis, including the influence of a transverse matrix cracking on the stress state of adjacent plies.

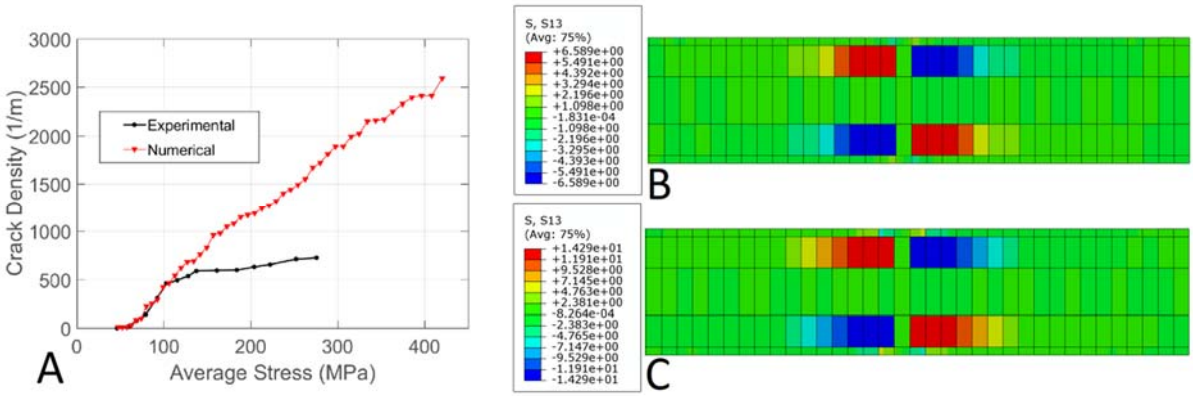

Fig. 18 – (A) Numerical experimental-correlation of crack density for the original modelling approach, (B) transverse shear stress close to a crack in the original model, and (C) with coupling between damage in the semi-phases

The application of Eq. 30 leads to an increment of the shear stress close to a matrix crack, depending on the value of the coupling parameter. In particular, with *h* equal to 1 the values are more than twice as large, as shown in Fig. 18-C. After the development of some cracks, the shear stress values exceed the assigned interlaminar strength, and delamination onset is predicted, as in Fig. 19-A. The increment of

the coupling parameter *h* involves a reduction of the crack density after an average stress of about 100 MPa, as shown in Fig. 19-B. Hence, the experimental evolution of the crack density can be captured once the constitutive law is calibrated in order to properly model the interaction between delamination and matrix cracking.

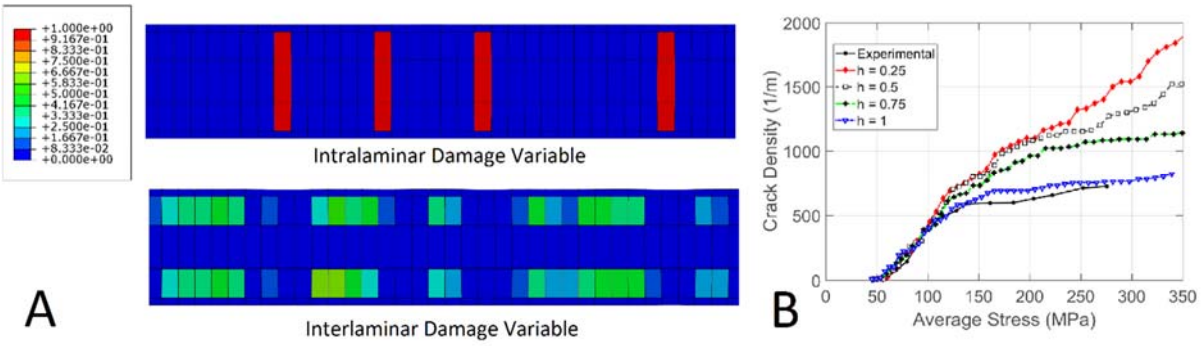

Fig. 19 – Effects of coupling between damage in matrix semi-phases: (A) intralaminar and interlaminar damage in a multiple transverse crack scenario, (B) numerical-experimental correlation of crack density for increasing values of the coupling parameter

A further improvement is introduced by modifying the law in order to model the interlaminar-intralaminar damage interaction at local level. In particular, the weakening of the interlaminar layer close to the tip of an intralaminar crack is taken into account. A variation of interlaminar strength and toughness is introduced, depending on the value of the intralaminar damage in the same matrix element. Such direct coupling is made possible by the specific characteristics of the bi-phasic modelling technique, and can be exploited in several ways. For the purpose to evaluate the effect on the crack density evolution in a pure tensile load condition, the simplified form expressed in Eq. 31 is adopted.

$$\begin{aligned} \sigma'_{I0} &= \sigma_{I0} \\ \sigma'_{II0} &= \sigma_{II0}\left(1 - max(d^U_{mc}, d^L_{mc})\right) \\ G'_I &= G_I \\ G'_{II} &= G_{II}\left(1 - max(d^U_{mc}, d^L_{mc})\right) \end{aligned} \qquad \text{Eq. 31}$$

The results obtained are summarized in Fig. 20. The magnified zone of the strip model shows four cracks and a complete interlaminar damage at the bottom and top crack ends, orginated by the coupling introduced through Eq. 31. Among the cracks, the matrix elements between the 0° and the 90° oriented

plies are partially delaminated due to the action of transverse shear stress. The crack density evolution curves shown in Fig. 20-B result lower than the one obtained through the coupling of the intralaminar damage in the matrix semi-phases, presented in Fig. 19-B. When the coupling parameter, h, is set at 1, the results reported in Fig. 20-B show that the introduction of Eq. 31 leads to a flat crack density vs. average stress curve. Accordingly, stress transfer mechanisms are totally inhibited by delamination and this opposes to the development of further cracks beyond a density level of 660 m^{-1}.

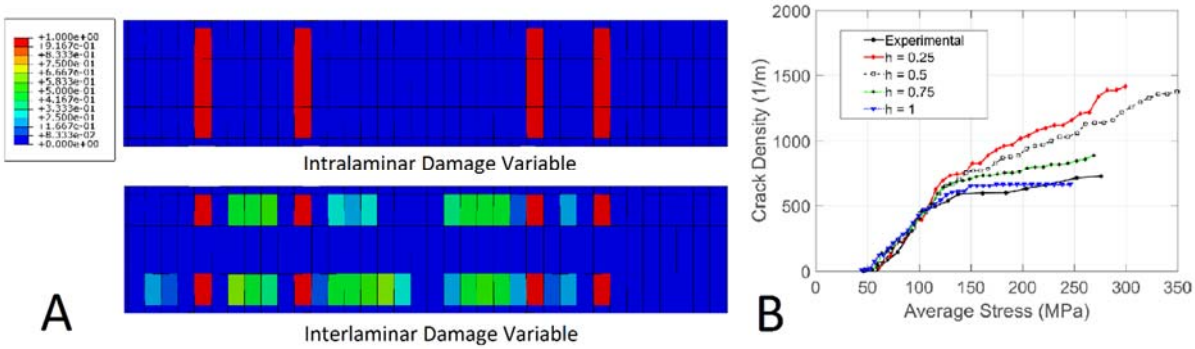

Fig. 20 – Effects of interaction between intralaminar damage and CZM for delamination: (A) modelling of multiple matrix cracking, (B) development of interlaminar damage, (C) numerical-experimental correlation of crack density evolution

Overall, the results obtained with a coupling parameter h =1 indicate that a good numerical-experimental correlation can be achieved. It has been shown that the bi-phasic modelling technique developed in this paper provides the possibility to act at different levels in order to model the effects of coupling between intralaminar and interlaminar damage without a representation of the stress field at the sub-ply level.

6. Concluding remarks

An innovative approach to model long fibre reinforced composite laminates has been developed by applying a decomposition of the composite into two phases, which model the fibre- and the matrix-dominated properties of the material. Such bi-phasic decomposition has been introduced within an efficient modelling technique developed to represent complex delamination scenarios, which had been presented and validated in previous works. The original technique was based on the embedment of a

CZM into finite thickness 3D elements, carrying only out-of-plane stress components. These elements connected elements with two-dimensional geometries, representing the whole in-plane response of the plies. In the new bi-phasic model presented in this paper, the fibre phase has been lumped at the mid-plane of the plies and it was represented by elements with two-dimensional geometry, whereas the complete three-dimensional stress-strain response of the matrix phase has been modelled through the 3D elements. The meshes of the two phases occupy the same volume and interact at the mid-plane of the plies. This approach, denominated bi-phasic modelling technique, provides the opportunity to embed a description of delamination in the element of the matrix in terms of relative displacement of the mid-planes of adjacent plies. Accordingly, a CZM can be introduced in finite thickness solid elements, with significant computational advantages, already proved in previous works. Besides such advantage, the main objective of the approach is to model both interlaminar and intralaminar damage mechanisms in the matrix within the same element, by using a single constitutive law.

Two basic issues have been addressed to develop the new approach. First, a new strategy was developed to decompose composite properties, fixing the issues of previous procedures relevant to the physical admissibility of the matrix phase. Then, the problems inherent the characterization of matrix elements has been considered. Such elements represent the matrix-dominated properties in the volume between two mid-planes of two different plies with different properties and/or orientations. The issue relating to the combination of the matrix-dominated responses of the two plies has been solved by conceiving a particular structure for the constitutive law of the matrix phase. Moreover, the law also allows to model large delamination openings between the semi-phases.

The capability to obtain a correct modelling delamination by means of the CZM embedded in the matrix elements has been successfully assessed in the paper by considering delamination tests in mode I and mode II. Such analyses have been also exploited to show that in-plane stress contributions attributed to the matrix phase are reliably modelled even in the presence of delamination cracks in the same element.

Moreover, computational advantages referred to the embedment of CZM into a finite thickness element have been confirmed through the comparison with conventional models.

The possibility to model in a reliable way both delamination and a matrix-dominated in-plane stress response in the same element opens appealing opportunities to model intralaminar damage and its potential interactions with delamination by using finite element schemes refined at the meso-scale level. Indeed, considering the development of transverse matrix cracking in cross-ply laminates, appreciable numerical-experimental correlations have been achieved. It has been shown that the approach can model individual intralaminar cracks with a minimum through-the-thickness mesh refinement level and that experimental crack density evolution can be appreciably captured by statistically distributing the matrix properties. Moreover, the load transfer mechanisms between adjacent damaged and undamaged plies can be properly modelled and controlled. This has given the possibility to capture the evolution of matrix cracks in an experimental case characterized by the interaction between delamination and transverse matrix cracking. The interaction was captured by properly calibrating the constitutive law attributed to the matrix, without relying on the detailed representation of the stress states at the crack tips and without requiring non-local approaches. The results suggest that the proposed approach can be considered a new and promising method to develop computationally efficient meso-scale models of laminates. They also suggest that such models can be used to simplify the representation of complicated phenomena and interactions originated by mechanisms occurring at a much smaller scale of observation.

References

[1] Schulte K, Stinchcomb WW. Damage Mechanisms - Including Edge Effects - in Carbon Fibre-reinforced Composite Materials. In: Friedrich K, editor. Compos. Mater. Ser., vol. 6, Elsevier; 1989, p. 273–324.

[2] Highsmith A, Reifsnider K. Stiffness-Reduction Mechanisms in Composite Laminates. In: Reifsnider K, editor. Damage Compos. Mater. Basic Mech. Accumul. Toler. Charact., 100 Barr Harbor Drive, PO Box C700, West Conshohocken, PA 19428-2959: ASTM International; 1982, p. 103-103–15.

[3] Hashin Z. Analysis of stiffness reduction of cracked cross-ply laminates. Eng Fract Mech 1986;25;(5–6):771–8.

[4] Berthelot J-M, Leblond P, El Mahi A, Le Corre J-F. Transverse cracking of cross-ply laminates: Part 1. Analysis. Compos Part A 1996;27;(10):989–1001.
[5] Nairn JA. 2.13 Matrix Microcracking in Composites, n.d., p. 34.
[6] Bolotin VV. Delaminations in composite structures: Its origin, buckling, growth and stability. Compos Part B Eng 1996;27;(2):129–45.
[7] MIL-HDBK-17-3F Military Handbook, Polymer matrix composite: Materials usage, design and analysis. vol. 3. US Department of Defense; 2002.
[8] Braga DFO, Tavares SMO, da Silva LFM, Moreira PMGP, de Castro PMST. Advanced design for lightweight structures: Review and prospects. Prog Aerosp Sci 2014;69:29–39.
[9] Maire JF, Chaboche JL. A New Formulation of Continuum Damage Mechanics (CDM) for Composite Materials. Aerosp Sci Technol 1997;1;(4):247–257.
[10] Ladeveze P, LeDantec E. Damage modelling of the elementary ply for laminated composites. Compos Sci Technol 1992;43;(3):257–67.
[11] Ladevèze P, Allix O, Deü J-F, Lévêque D. A mesomodel for localisation and damage computation in laminates. Comput Methods Appl Mech Eng 2000;183;(1–2):105–22.
[12] Maimí P, Camanho PP, Mayugo JA, Dávila CG. A continuum damage model for composite laminates: Part I – Constitutive model. Mech Mater 2007;39;(10):897–908.
[13] Maimí P, Camanho PP, Mayugo JA, Dávila CG. A continuum damage model for composite laminates: Part II – Computational implementation and validation. Mech Mater 2007;39;(10):909–19.
[14] Lubineau G, Ladevèze P. Construction of a micromechanics-based intralaminar mesomodel, and illustrations in ABAQUS/Standard. Comput Mater Sci 2008;43;(1):137–145.
[15] Maimi P, Mayugo JA, Camanho PP. A Three-dimensional Damage Model for Transversely Isotropic Composite Laminates. J Compos Mater 2008;42;(25):2717–2745.
[16] Abisset E, Daghia F, Ladevèze P. On the validation of a damage mesomodel for laminated composites by means of open-hole tensile tests on quasi-isotropic laminates. Compos Part A 2011;42;(10):1515–1524.
[17] Pinho ST, Iannucci L, Robinson P. Physically-based failure models and criteria for laminated fibre-reinforced composites with emphasis on fibre kinking: Part I: Development. Compos Part Appl Sci Manuf 2006;37;(1):63–73.
[18] Pinho ST, Iannucci L, Robinson P. Physically based failure models and criteria for laminated fibre-reinforced composites with emphasis on fibre kinking. Part II: FE implementation. Compos Part Appl Sci Manuf 2006;37;(5):766–77.
[19] Farrokhabadi A, Hosseini-Toudeshky H, Mohammadi B. Damage analysis of laminated composites using a new coupled micro-meso approach. Fatigue Fract Eng Mater Struct 2010;33;(7):420–35.
[20] Mohammadi B, Rohanifar M, Salimi-Majd D, Farrokhabadi A. Micromechanical prediction of damage due to transverse ply cracking under fatigue loading in composite laminates. J Reinf Plast Compos 2017;36;(5):377–95.
[21] De Rouvray A, Haugh E. Failure of brittle and composite materials by numerical methods. In: Wierzbicki T, editor. Struct. Fail., New York: Wiley; 1989, p. 193–254.
[22] Haugh E, De Rouvray A. Crash response of composite structures. In: Jones N, Wierzbicki T, editors. Struct. Crashworthiness Fail., Elsevier; 1993, p. 237–94.

[23] Coutellier D, Rozycki P. Multi-layered multi-material finite element for crashworthiness studies. Compos Part A 2000;31;(8):841–851.
[24] Airoldi A, Baldi A, Mostosi V, Sala G. A Bi-Phasic Approach to Model Progressive Matrix Damage in Composites: Development and Application, Venice: 2012.
[25] Dzenis YA, Qian J. Analysis of microdamage evolution histories in composites. Int J Solids Struct 2001;38;(10):1831–54.
[26] Cox BN, Carter WC, Fleck NA. A binary model of textile composites—I. Formulation. Acta Metall Mater 1994;42;(10):3463–79.
[27] Xu J, Cox BN, McGlockton MA, Carter WC. A binary model of textile composites—II. The elastic regime. Acta Metall Mater 1995;43;(9):3511–24.
[28] Flores S, Evans AG, Zok FW, Genet M, Cox B, Marshall D, et al. Treating matrix nonlinearity in the binary model formulation for 3D ceramic composite structures. Compos Part Appl Sci Manuf 2010;41;(2):222–9.
[29] Wisnom MR. Modelling discrete failures in composites with interface elements. Compos Part Appl Sci Manuf 2010;41;(7):795–805.
[30] Corigliano A. Formulation, identification and use of interface models in the numerical analysis of composite delamination. Int J Solids Struct 1993;30;(20):2779–811.
[31] Camanho PP, Davila CG, de Moura MF. Numerical Simulation of Mixed-Mode Progressive Delamination in Composite Materials. J Compos Mater 2003;37;(16):1415–38.
[32] Schellekens JCJ, De Borst R. On the numerical integration of interface elements. Int J Numer Methods Eng 1993;36;(1):43–66.
[33] de Borst R, Remmers JJC. Computational modelling of delamination. Compos Sci Technol 2006;66;(6):713–22.
[34] Turon A, Dávila CG, Camanho PP, Costa J. An engineering solution for mesh size effects in the simulation of delamination using cohesive zone models. Eng Fract Mech 2007;74;(10):1665–82.
[35] Airoldi A, Sala G, Bettini P, Baldi A. An efficient approach for modeling interlaminar damage in composite laminates with explicit finite element codes. J Reinf Plast Compos 2013;32;(15):1075–1091.
[36] Airoldi A, Baldi A, Bettini P, Sala G. Efficient modelling of forces and local strain evolution during delamination of composite laminates. Compos Part B Eng 2015;72:137–49.
[37] Wagner W, Balzani C. Simulation of delamination in stringer stiffened fiber-reinforced composite shells. Comput Struct 2008;86;(9):930–9.
[38] Balzani C, Wagner W. An interface element for the simulation of delamination in unidirectional fiber-reinforced composite laminates. Eng Fract Mech 2008;75;(9):2597–615.
[39] Balzani C, Wagner W, Wilckens D, Degenhardt R, Büsing S, Reimerdes H-G. Adhesive joints in composite laminates—A combined numerical/experimental estimate of critical energy release rates. Int J Adhes Adhes 2011.
[40] Mohammadi B, Salimi-Majd D. Investigation of delamination and damage due to free edge effects in composite laminates using cohesive interface elements. Eng Solid Mech 2014;2;(2):101–18.

[41] Baldi A, Airoldi A, Crespi M, Iavarone P, Bettini P. Modelling competitive delamination and debonding phenomena in composite T-Joints. Procedia Eng 2011;10:3483–9.
[42] Baldi A, Airoldi A, Crespi M, Giuseppe Nettuno P, Sala G. Numerical Evaluation of the Compressive Residual Strength in Impact-Damaged Composite Laminates, Venice: 2011.
[43] Baldi A, Airoldi A, Belotti P, Bettini P, Sala G. Numerical and Experimental Analyses of Multiple Delaminations in Curved Composite Laminates, Montreal: 2013.
[44] Airoldi A, Baldi A, Corio M, Fanteria D, Lazzeri L, Mariani U, et al. Improved Methodology for the Design of Damage Tolerant Helicopter Structures in Composite Materials, Jerusalem: 2013.
[45] Aymerich F, Dore F, Priolo P. Prediction of impact-induced delamination in cross-ply composite laminates using cohesive interface elements. Compos Sci Technol 2008;68;(12):2383–90.
[46] Kumar D, Roy R, Kweon J-H, Choi J. Numerical Modeling of Combined Matrix Cracking and Delamination in Composite Laminates Using Cohesive Elements. Appl Compos Mater 2016;23;(3):397–419.
[47] Hallett SR, Jiang W-G, Khan B, Wisnom MR. Modelling the interaction between matrix cracks and delamination damage in scaled quasi-isotropic specimens. Compos Sci Technol 2008;68;(1):80–9.
[48] Berthelot J-M, Le Corre J-F. Statistical analysis of the progression of transverse cracking and delamination in cross-ply laminates. Compos Sci Technol 2000;60;(14):2659–2669.
[49] Wisnom MR, Hallett SR. The role of delamination in strength, failure mechanism and hole size effect in open hole tensile tests on quasi-isotropic laminates. Compos Part Appl Sci Manuf 2009;40;(4):335–42.
[50] Abisset E, Daghia F, Sun XC, Wisnom MR, Hallett SR. Interaction of inter- and intralaminar damage in scaled quasi-static indentation tests: Part 1 – Experiments. Compos Struct 2016;136:712–26.
[51] Li W, Jia Y, Li L. A Two-Scale Approach to Numerically Predict the Strength and Degradation of Composites. Appl Compos Mater 2017;25.
[52] van Der Meer FP, Dávila CG. Cohesive modeling of transverse cracking in laminates under in-plane loading with a single layer of elements per ply. Int J Solids Struct 2013;50;(20–21):3308–3318.
[53] Iarve EV. Mesh independent modelling of cracks by using higher order shape functions. Int J Numer Methods Eng 2003;56;(6):869–82.
[54] Sun W, Guan Z, Li Z. Simulation of Low Velocity Impact Induced Inter- and Intra-Laminar Damage of Composite Beams Based on XFEM. Appl Compos Mater 2017;24;(6):1459–77.
[55] Sun XC, Wisnom MR, Hallett SR. Interaction of inter- and intralaminar damage in scaled quasi-static indentation tests: Part 2 – Numerical simulation. Compos Struct 2016;136;(Supplement C):727–42.
[56] Shi Y, Soutis C. Modelling transverse matrix cracking and splitting of cross-ply composite laminates under four point bending. Theor Appl Fract Mech 2016;83:73–81.
[57] Mohammadi B, Olia H, Hosseini-Toudeshky H. Intra and damage analysis of laminated composites using coupled continuum damage mechanics with cohesive interface layer. Compos Struct 2015;120:519–530.

[58] MIL-HDBK-17-2E Military Handbook, Polymer matrix composite: Materials properties. US Department of Defense; 1999.
[59] Jones RM. Mechanics of composite materials. 2nd ed. Philadelphia, PA: Taylor and Francis; 1999.
[60] Lagarias JC, Reeds JA, Wright MH, Wright PE. Convergence Properties of the Nelder--Mead Simplex Method in Low Dimensions. SIAM J Optim 1998;9;(1):112–47.
[61] Benzeggagh ML, Kenane M. Measurement of mixed-mode delamination fracture toughness of unidirectional glass/epoxy composites with mixed-mode bending apparatus. Compos Sci Technol 1996;56;(4):439–49.
[62] Simo JC, Ju JW. Strain- and stress-based continuum damage models—I. Formulation. Int J Solids Struct 1987;23;(7):821–40.
[63] Laws N, Dvorak GJ. Progressive Transverse Cracking In Composite Laminates. J Compos Mater 1988;22;(10):900–16.
[64] Abaqus®. 6.10 Documentation. Analysis User's Guide, Volume IV: Elements. Providence (RI, USA): Dassault Systemes Simulia Corp.; 2010.
[65] ASTM D5528 - 13, Standard Test Method for Mode I Interlaminar Fracture Toughness of Unidirectional Fiber-Reinforced Polymer Matrix Composites. ASTM International; n.d.
[66] Carlsson LA, Gillespie JW. Chapter 4 - Mode-II Interlaminar Fracture of Composites. In: Friedrich K, editor. Compos. Mater. Ser., vol. 6, Elsevier; 1989, p. 113–57.
[67] Daudeville L, Allix O, Ladevèze P. Delamination analysis by damage mechanics: Some applications. Compos Eng 1995;5;(1):17–24.
[68] Feng W, Reifsnider K, Sendeckyj G, Chiao T, Rodericks G, Stinchcomb W, et al. Fracture Mechanics of Sublaminate Cracks in Composite Materials. J Compos Technol Res 1984;6;(2):45.
[69] Manders PW, Chou T-W, Jones FR, Rock JW. Statistical analysis of multiple fracture in 0°/90°/0° glass fibre/epoxy resin laminates. J Mater Sci 1983;18;(10):2876–89.